LIQUEFACTION POTENTIAL MAP
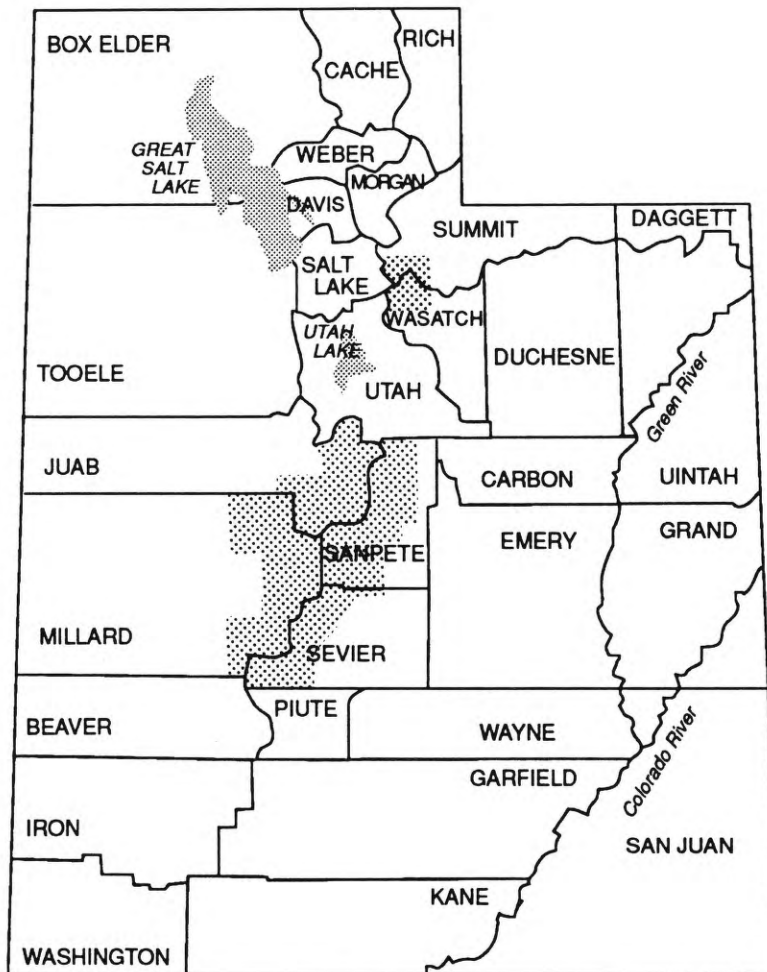# FOR CENTRAL UTAH
COMPLETE TECHNICAL REPORT

by
Loren R. Anderson
Jeffrey R. Keaton
John D. Rice

LIQUEFACTION POTENTIAL MAP

for

CENTRAL UTAH

by

Loren R. Anderson
Jeffrey R. Keaton
John D. Rice

Department of Civil and Environmental Engineering
Utah State University
Logan, Utah

March, 1990

LIQUEFACTION POTENTIAL MAP

for

CENTRAL, UTAH

by

Loren R. Anderson, Principal Investigator
Jeffrey R. Keaton, Co-Principal Investigator
John D. Rice

Department of Civil and Environmental Engineering
Utah State University
Logan, Utah 84322-4100

The views and conclusions contained in this document are those of the authors and should not be interpreted as necessarily representing the official policies, either expressed or implied, of the U. S. Government.

ACKNOWLEDGEMENTS

TABLE OF CONTENTS

TABLE OF CONTENTS (continued)

TABLE OF CONTENTS (continued)

TABLE OF CONTENTS (continued)

LIST OF TABLES

LIST OF FIGURES

LIST OF FIGURES (continued)

LIST OF FIGURES (continued)

LIST OF PLATES

INTRODUCTION

Problem Statement

<u>General</u>

In 1964, the civil engineering community was forced to recognize soil liquefaction due to seismic shaking as a very important geologic hazard. During 1964, two major earthquakes occurred (one in Niigata, Japan and the other in Anchorage, Alaska) in which substantial damages were attributed to liquefaction. In Niigata alone, most of the over $1 billion in damages can be attributed to liquefaction-type failures (National Research Council, 1985), and in the Anchorage earthquake 60 percent of the estimated $300 million in damages were the result of liquefaction (Youd, 1978). Although liquefaction failures have occurred in almost all large earthquakes, both preceding and following 1964, the events of that year sparked interest in liquefaction research that continues today. In the 26 years since 1964, much research has been conducted in order to better understand the liquefaction process and to develop appropriate technologies for dealing with the hazard.

Soil liquefaction is described by Youd (1973) as the transformation of a granular material from a solid state into a liquefied state as a consequence of increased pore-water pressure. Many mechanisms for liquefaction-induced ground failure have been identified; however, all of the mechanisms can be grouped into one of three general types: 1) bearing capacity failure, 2) lateral spread failure, and 3) flow landslide. The

type of mechanism depends mostly on the slope of the ground and, to a lesser degree, the depth and thickness of the liquefied layer (Youd, 1978).

Purpose

The general public, its governing agencies and other groups associated with the zoning and development of land and structures typically have a poor understanding of the liquefaction phenomena. The lack of understanding is not restricted to knowing where and how liquefaction is likely to occur, but often people are unaware that this type of hazard exists. Therefore, the public, its agencies and its businesses need to be informed of the hazard and a tool needs to be provided to aid in the assessment of the associated risk.

The purpose of this study is to provide the tool for evaluating the liquefaction hazard. This tool is in the form of liquefaction potential maps that can be used to delineate areas in which liquefaction is likely to be a hazard. The hazard can then be evaluated and dealt with in the manner compatible with codes and accepted practice.

Objective

Continuing with the ongoing research in liquefaction mapping along the Wasatch Front in Utah, the main objective of this study was to produce liquefaction potential maps for the Central Utah area. In this study, many fewer data were available and a much larger study area was covered than in the previous four projects. Therefore, a secondary

objective was to deal with the special problems associated with scarce data and to amend the procedure used in the previous studies to account for these problems.

Scope

The scope of this study was to evaluate the liquefaction potential in the populated alluvial valleys of Juab, Millard, Sanpete and Sevier Counties and the Park City-Heber area in Wasatch and Summit counties. The evaluation was based on subsurface data, Quaternary geology of the area, and the seismicity of the region. Subsurface data, in the form of boring logs, were collected from local consulting firms and government agencies and supplemented with a field investigation conducted as part of the study. Geologic and groundwater information was collected from published reports and field reconnaissance. The seismicity of the region was evaluated as part of this study.

Study Area

Location

The location of the study area is shown on Figure 1. It consists of the populated areas of Juab, Millard, Sanpete and Sevier Counties along with the Park City-Heber area, which lies in Summit and Wasatch counties. The lower section of the study area is bounded on the west by the Basin and Range Province and on the east by the Wasatch Plateau. The Park City-Heber area is located within the Wasatch Range approximately 20 miles east of Salt Lake City.

4
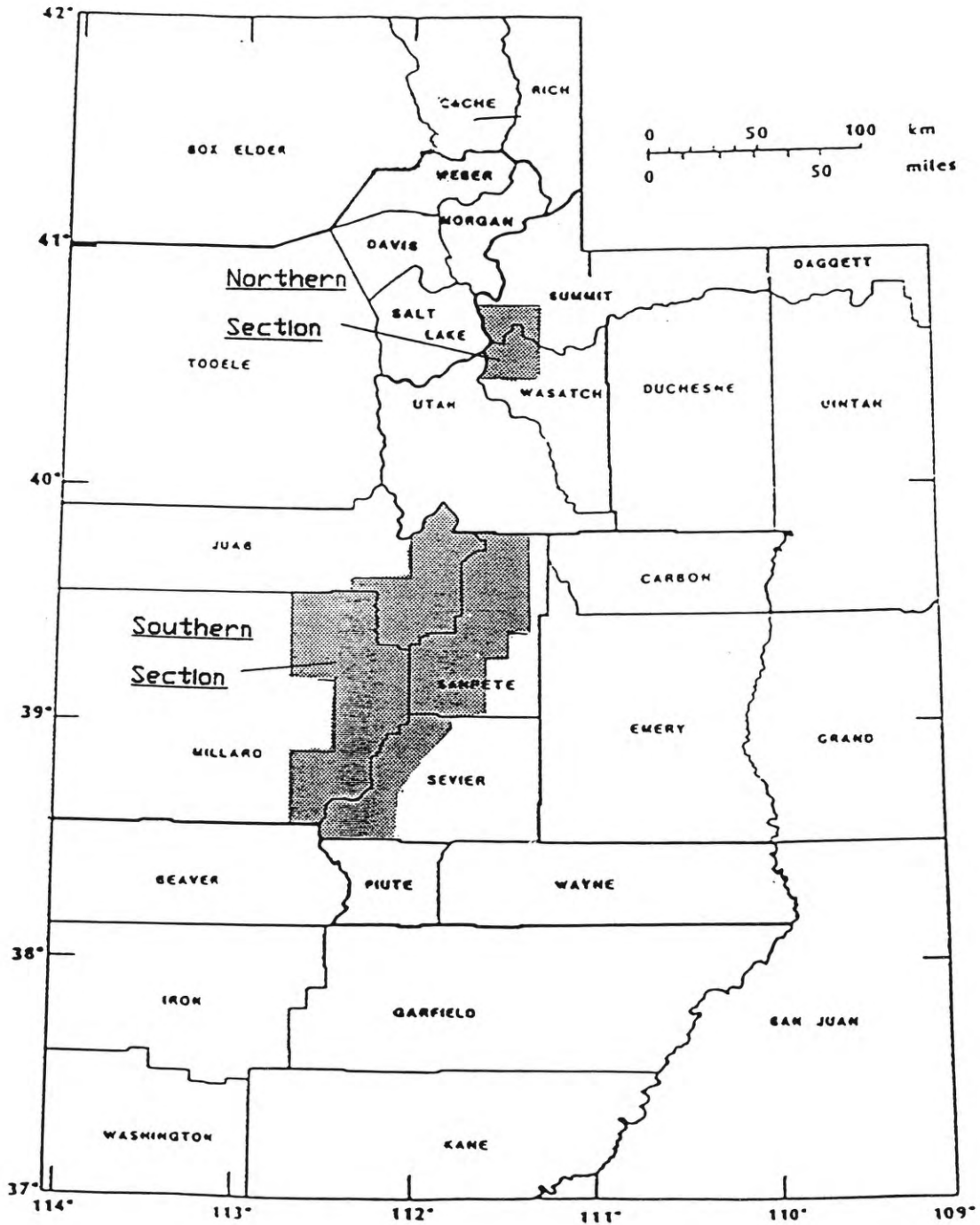
Figure 1. Map showing general location of northern and southern sections of study area.

The area includes several small cities and towns. The largest city in the study areais Richfield in Sevier County with a population of 5482 (1980 Census). Other cities in the study area include Park City and Heber in Wasatch and Summit counties, Nephi in Juab County, Delta and Fillmore in Millard County, Manti and Ephraim in Sanpete County, Salina in Sevier County and numerous other small communities.

Geology

The present state of Central Utah is the result of an uplifting and block faulting process that began approximately 25 million years ago in the Miocene Epoch and continues today (Hintze, 1973). The mountains were formed by blocks uplifted along faults and the valleys formed on the downthrown sides of the faults. The valleys were contemporaneously filled with sediment from the adjacent eroding mountains.

About 16,000 years ago Lake Bonneville reached its highest elevation. In the study area, this high stand left shorelines at an elevation of approximately 5100 feet. It is worth noting that shorelines corresponding to this same lake level are found along the Wasatch Front at an elevation of approximately 5200 feet and on the Oquirrh Mountains at over 5300 feet. The variation in shoreline elevation is due to a doming action caused by isostatic rebound raising the center of the basin more than the outer fringes (Crittenden, 1963). During the high stand, a significant portion of the study area was inundated by the lake (Figure 2). Areas affected by sedimentation from Lake Bonneville include:
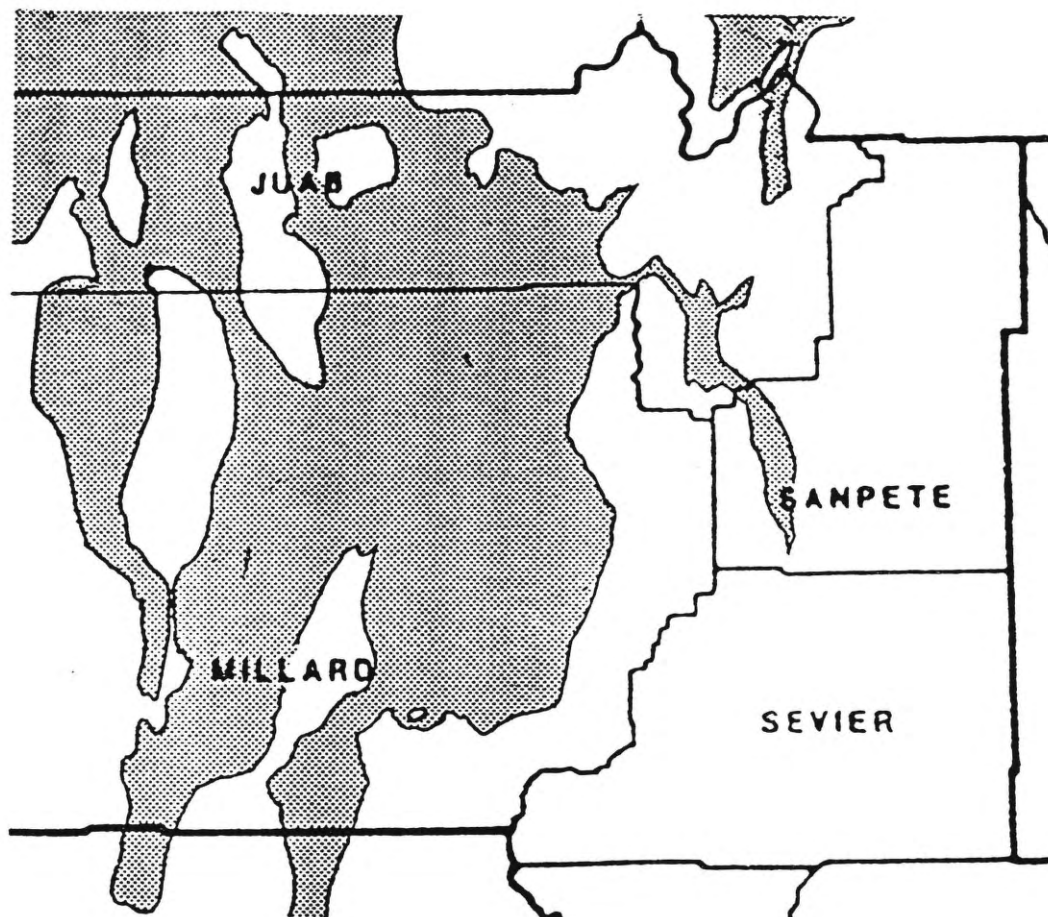
Figure 2. Map of the lower section of the study area showing the extent of Lake Bonneville at its highest level (Crittenden, 1963).

Northern Juab Valley, Northern Sevier Valley, Mills Valley and the Sevier Desert area (Hintze,1973; Crittenden,1963).

The unconsolidated sediments of the study area can be grouped into three general groups. The oldest of these sediments are the pre-Lake Bonneville deposits and old alluvium. This material is mainly of late Pleistocene age or older and is generally dense and cemented and, therefore, not susceptible to liquefaction.

The next group consists of the Lake Bonneville sediments. These sediments have a wide range of susceptibility to liquefaction depending on the local groundwater conditions and the soil types.

The third group is the young alluvium deposited on top of Lake Bonneville sediments or at an elevation above the Bonneville shorelines. They range in age from late Pleistocene to Holocene. They are the result of fluvial processes and are expressed as alluvial fans, stream and river channels and flood-plains. This group also will have a wide range of liquefaction susceptibilities.

The locations of the alluvial valleys in the lower portion of the study area are shown in Figure 3. The geology of these specific valleys is discussed in the following sections.

8
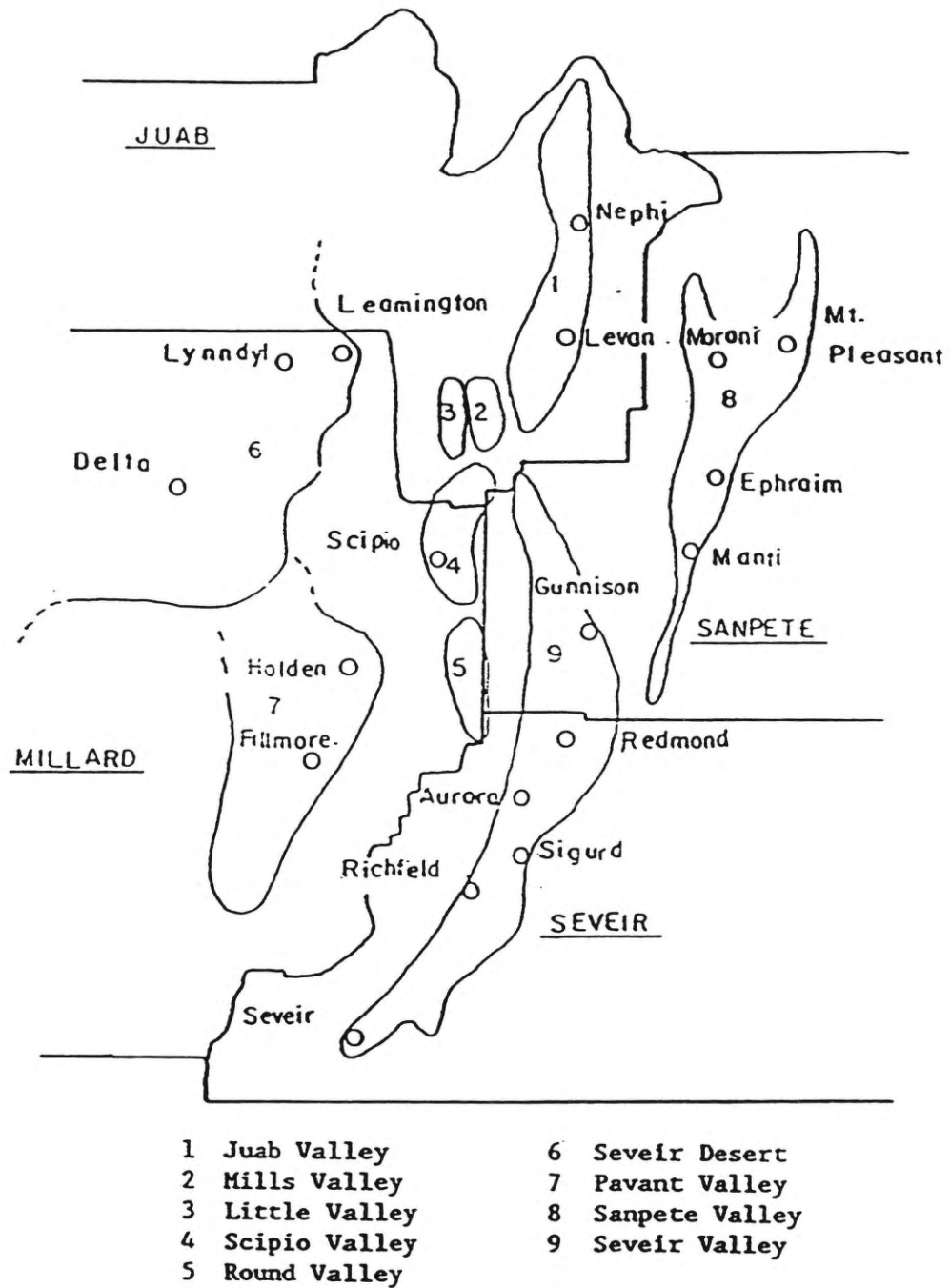
Figure 3. Map of the alluvial valleys of the southern section of the study area.

1 Juab Valley
2 Mills Valley
3 Little Valley
4 Scipio Valley
5 Round Valley
6 Seveir Desert
7 Pavant Valley
8 Sanpete Valley
9 Seveir Valley

Juab Valley. The Juab Valley is a structural trough formed between the Wasatch fault to the east and eastward- dipping layers of bedrock underlying the valley and bounding it to the west. The valley is separated into two basins by Levan Ridge, located five miles south of Nephi. Levan Ridge also acts as a north-south groundwater divide between the two basins (Bjorklund, 1967).

The valley fill of northern Juab Valley generally consists of alluvial fan, lacustrine and flood-plain deposits. With the exception of isolated recent deposits, the lacustrine deposits are the result of the high stand of Lake Bonneville. Around the margins of the valley, alluvial fans interfinger with and overlie the lacustrine deposits. The alluvial fans generally consist of coarse gravel at the valley edges and become progressively finer toward the center of the valley. Flood-plain deposits are found adjacent to the small creeks in the center of the valley (Bjorklund, 1967).

Southern Juab Valley was not inundated by Lake Bonneville except for a small area around Chicken Creek Reservoir. Therefore, the valley fill is dominated by large alluvial fans extending westward across the valley floor from the San Pitch Mountains. In the central and southwestern parts of the valley minor, flood-plain and lacustrine deposits exist along with the alluvial fans (Bjorklund and Robinson, 1968).

Scipio, Round, Little and Mills Valleys. Scipio, Round, Little and Mills Valleys represent a graben basin on the western side of the Pavant Range. Although Little and Mills Valleys are not entirely within the graben, their structure is very similar to that of

Scipio and Round Valleys (Bjorklund and Robinson, 1968).

Scipio, Round and most of Little Valley are above the Bonneville Shoreline and are, therefore, dominated by alluvial fan material. There are also scattered lacustrine and flood-plain deposits. Mills Valley and the lower elevations of Little Valley, on the other hand, are dominated by Lake Bonneville deposits and deposits of the Sevier River flood-plain (Bjorklund and Robinson, 1968; Meinzer, 1911).

Sevier Desert. The Quaternary deposits of the Sevier Desert are the result of a complex interaction of lacustrine, fluvial, eolian and alluvial processes. The oldest unconsolidated sediments were deposited by an interactive process between Lake Bonneville and the Sevier River. As the lake rose and fell to different elevations, the Sevier River supplied sediments to be worked and reworked into a complex system. This system is composed of lake bottom and shoreline deposits as well as deltaic deposits at several different levels. As Lake Bonneville subsided, the Sevier River meandered over a width of 20 miles as it weaved its way to the Sevier Lake Basin, reworking the previously deposited Lake Bonneville sediments into flood-plain and other related fluvial deposits. The latter process continues today as evidenced by the numerous abandoned meander belts and oxbow lakes (Mower and Feltis, 1968; Eardley et al., 1957; Meinzer, 1911).

The result of the Lake Bonneville-Sevier River interaction is a complex system of interbedded and interfingering deposits varying from gravel to clay. Generally, the

deposits are coarsest at the mouth of Sevier Canyon, near Leamington, and become progressively finer toward the southwest and west (Mower and Feltis, 1968).

Overlying the Lake Bonneville deposits in some areas are deposits of more recent processes. At the margins of the mountains surrounding the desert are alluvial fan deposits. These deposits are of late Pleistocene age. West of Delta lies a large field of recent sand dunes. This deposit reaches from ten miles north of Lynndyl and continues south through the Pavant Valley. A number of playa deposits are also scattered throughout the desert floor due to marshy areas and the Sevier Lake bed (Mower and Feltis, 1968).

Pavant Valley. The Pavant Valley is bounded on the east by the Pavant Range and to the west by a number of low-lying volcanic mesas. To the northeast the valley is open and leads into the Sevier Desert. A large alluvial slope extends from the Pavant Range and descends gradually across the valley to the mesas and flat lands. Lake Bonneville occupied the lower elevations of the valley and left a distinct shoreline on the alluvial slope that passes through Holden and Fillmore (Meinzer, 1911).

Sanpete Valley. Two major structural elements form the Sanpete Valley. The Sevier fault forms the western boundary of the valley and, likewise, the San Pitch Mountains on the upthrown side of the fault. The east side of the valley is formed by the western boundary of the Wasatch Plateau which is a west-dipping monocline (Robinson, 1971).

The valley fill consists of alluvial fan, flood-plain and lacustrine deposits unrelated to Lake Bonneville. Alluvial fan deposits dominate the outer edges of the valley and are generally coarse gravel and cobbles near the valley sides becoming progressively finer toward the center of the valley. The central part of the valley, especially between Manti and Ephraim, is dominated by flood-plain and lacustrine deposits. The flood-plain and lacustrine deposits are generally fairly continuous where the alluvial deposits tend to be more lenticular and interfingered (Robinson, 1971).

Sevier Valley. The Sevier Valley is formed in a graben basin. The basin is bounded on the east by the Sevier fault. This section of the Sevier fault can be traced from northern Arizona to the vicinity of Sigurd. To the west the basin is bounded by the Elsinore fault from Elsinore to Aurora. Several other small unnamed faults also exist in the basin (Young and Carpenter, 1965).

The Sevier Formation of late Tertiary or early Quaternary age underlies the entire Sevier Valley and often crops out along the valley margins. The formation is a fanglomerate consisting of poorly sorted alluvial fan deposits ranging in particle size from boulders to silt. The deposits are generally quite dense and cemented (Young and Carpenter, 1965).

Overlying the Sevier River Formation is the typical valley sequence found throughout the study area consisting of alluvial fans, lacustrine and flood-plain deposits. Alluvial fans extend from the mouths of canyons and grade from coarse gravel to fine

sand toward the center of the valley. The central areas of the valley from Sevier to Redmond and North of Gunnison are dominated by well-sorted stream deposits laid down by the Sevier River. Lacustrine deposits are found in the valley bottoms around Redmond and northwest of Gunnison in the Sevier Bridge Reservoir area. The lakes in the Redmond area were formed behind the high bedrock of the Redmond Anticline while the Sevier Bridge Reservoir deposits are of Lake Bonneville origin (Crittenden, 1963; Young and Carpenter, 1965).

Park City-Heber area. The Park City-Heber area consists of two mountain valleys and the upper Provo Canyon. The Quaternary deposits in the area are, for the most part, due to alluvial, glacial and stream deposits and generally quite coarse grained. In most cases the valley fill consists of gravel, cobbles and boulders with a matrix of finer deposits, however, there are several fine grained deposits encountered in the Park City area. The northwest corner of the Heber Valley also contains extensive tufa deposits formed by the precipitation of carbonate from hot mineral water (Baker, 1970).

<u>Seismicity</u>

The study area is situated within the Intermountain Seismic Belt which runs north and south through Utah (Arabasz et al., 1979). Figure 4 shows the epicenters and magnitudes of earthquakes that occurred in Utah between July 1962 and June 1978. One can easily trace the Intermountain Seismic belt by noting the north-trending concentration of epicenters.

Figure 5 shows the locations of the many Quaternary faults in Utah. The Wasatch fault accounts for most of the seismic risk in the area, especially in Juab Valley and Sevier Valley north of Gunnison. The segments of the Wasatch fault that lie in the study area are capable of producing earthquakes of Richter magnitude 6.5 to 7.25 (Young et al., 1987). The fault as a whole is considered to have a recurrence interval of 250 to 280 years (Machette et al., 1987). Other large faults in the area include the Sevier fault and the Elsinore fault, both in south Sevier Valley. Although both of these faults are large enough to produce earthquakes above magnitude 7.0, no evidence is known which suggests that earthquakes larger than the 6.0 to 6.5 magnitude range have a reasonable probability of occurring north of Richfield. South of Richfield the area is adjacent to the central part of the Sevier fault which is thought to be more active. Thus, for the Sevier Valley south of Richfield a magnitude of 7.0 earthquake has a reasonable probability of occurring (Arabaz, 1988; Anderson, 1988).
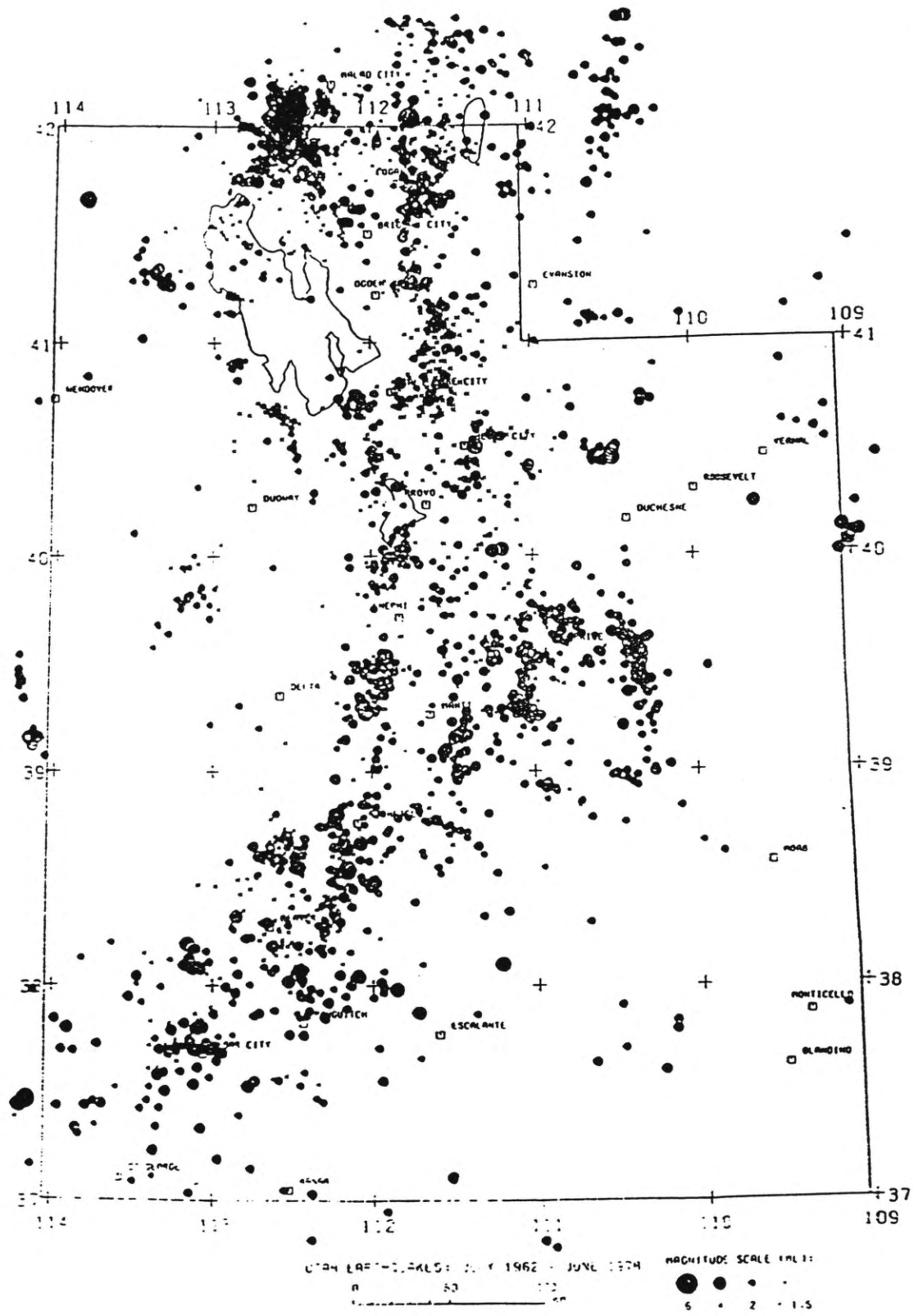
Figure 4. Locations of earthquake epicenters in Utah, July 1962 to July 1978 (after Arabasz et al., 1979).

16
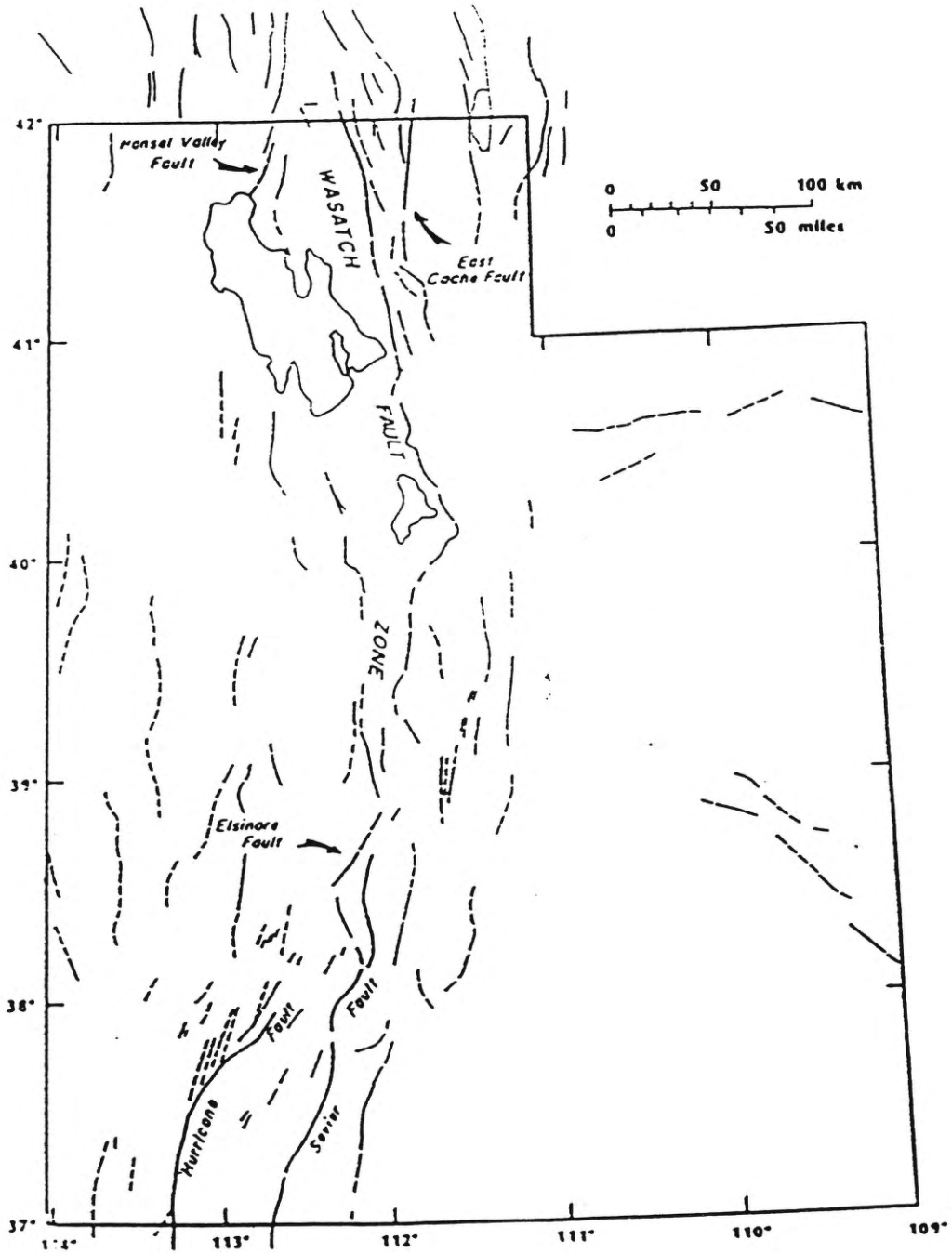
Figure 5. Quarternary faults identified in Utah (after Anderson and Miller, 1979).

In most locations of the study area (all except Juab, Little and Mills Valleys and Sevier Valley north of Gunnison) the background seismicity is responsible for most of the seismic risk. Background seismicity is not associated with faults considered capable of producing surface rupture. The largest magnitudes from these earthquakes range from 6.0 to 6.5 (Young et al.,1987).

LITERATURE REVIEW

Mechanisms of Liquefaction

General mechanism

Liquefaction occurs when saturated cohesionless soils experience shear straining. If the pore water was allowed to drain, the soil would undergo consolidation due to the rearrangement of soil grains during straining. Since, in many cases, the pore water is not allowed to drain freely, the soil does not consolidate; instead the overburden pressure is shifted from the soil grains to the pore water. The result is a pore water pressure increase. When the pore water pressure builds to the point where it is equal to the overburden pressure, the effective stress becomes zero and the soil looses its strength.

Behavior of sands during cyclic shear strain

When a loose sand is subjected to repeated back-and-forth straining (cyclic shear straining), the soil particles tend to rearrange into a denser configuration. Figure 6 shows the decrease in void ratio that can occur in a loose sand during cyclic loading. The rate at which this decrease takes place is strongly influenced by the magnitude of the cyclic strain (Youd, 1972). Dobry et al. (1981) showed that no densification will occur if strains are less than about 0.01 percent. This value has been called the threshold strain.
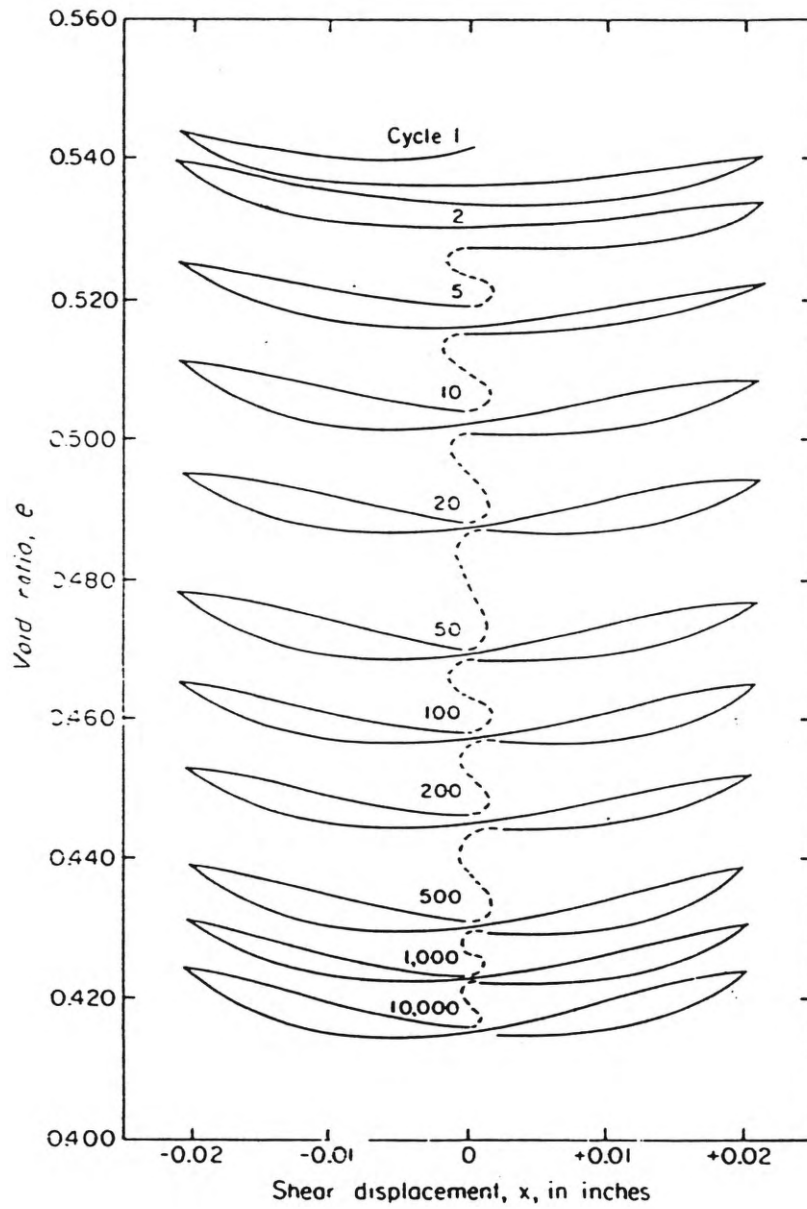
Figure 6. Void ratio versus cyclic shear displacement showing densification of a sand during cyclic loading (after Youd, 1972).

Pore pressure buildup during undrained cyclic loading

If the sand undergoing cyclic shear strain is saturated and drainage of the fluid is prevented, a decrease in volume is not possible. Instead of densifying the overburden stress on the soil is shifted from the sand grains to the pore water. This causes an increase in the pore water pressure while the overburden pressure remains constant. The result is a decrease in the intergranular effective stress. This process is shown schematically in Figure 7. The void ratio of the soil in Figure 7 would tend to decrease from point A to point B due to densification during cyclic loading if the pore water was allowed to drain. However, since the void ratio is held constant, the rebound curve is followed to determine the change in effective stress necessary to maintain the soil at the constant void ratio. The decrease in effective stress is compensated for by an increase in pore water pressure.

With continued cyclic loading the pore water pressure will continue to rise until it reaches the value of the overburden stress. At this point the effective stress will be zero and the soil's internal strength will have diminished. This condition is referred to as 100 percent pore pressure ratio (ASCE, 1978). Seed and Lee (1966) demonstrated this process with cyclic triaxial tests. Some of the results of these tests are shown in Figure 8.
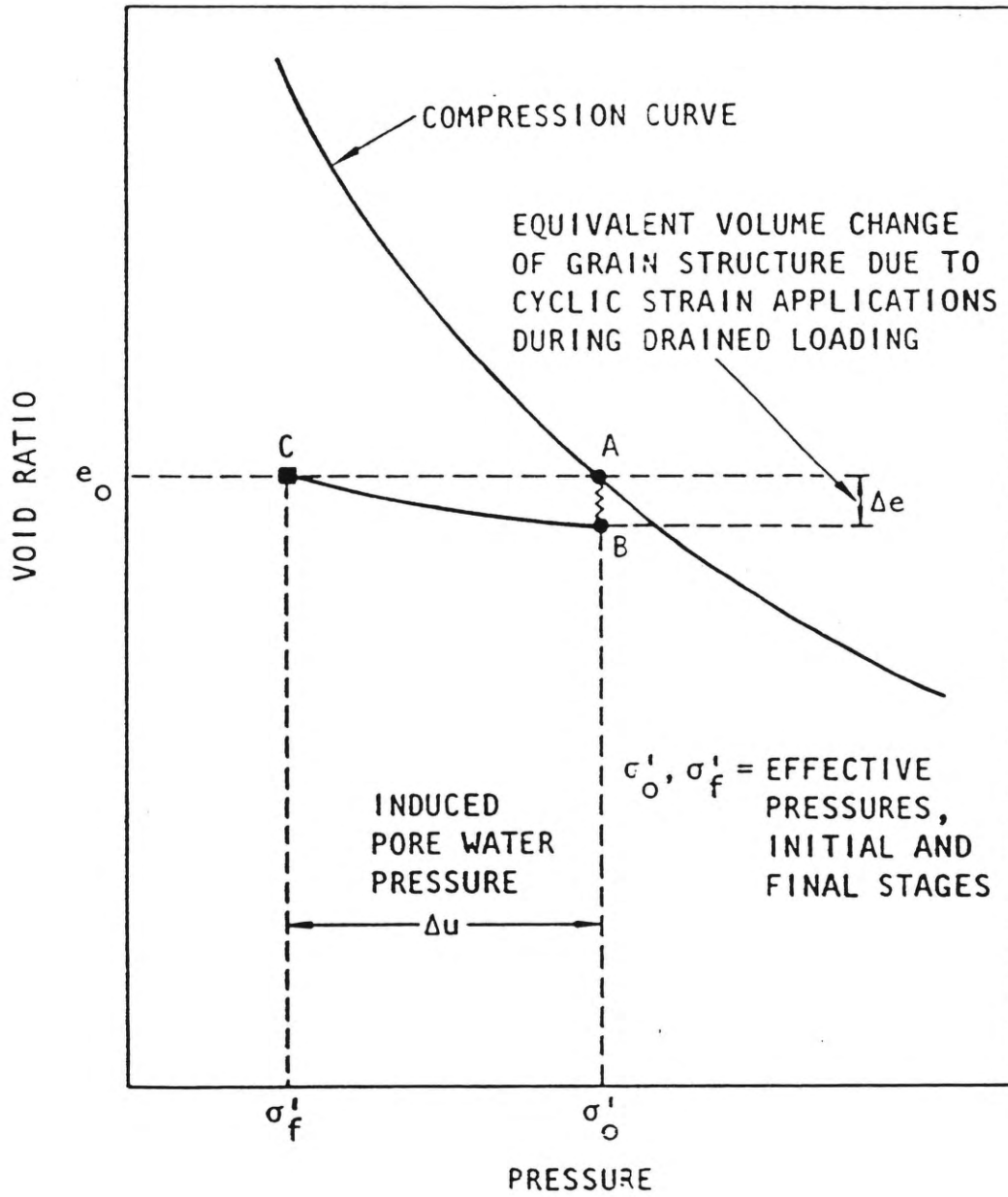
Figure 7. Schematic illustration of pore pressure generation (after Seed, 1979).
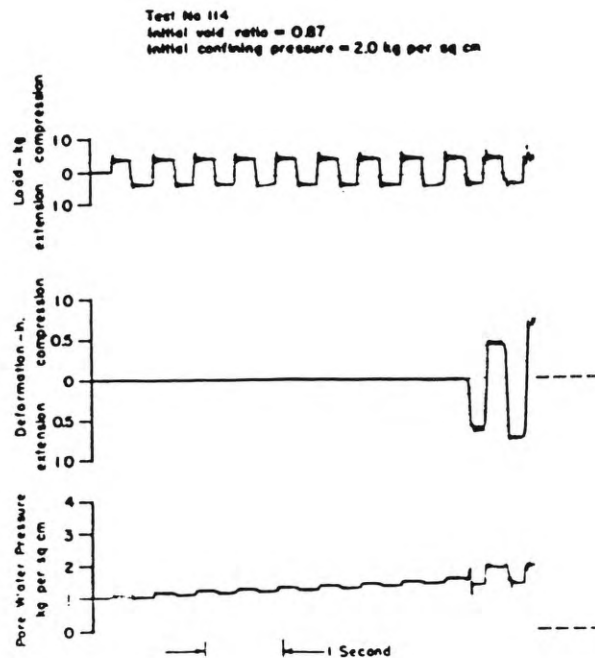
Figure 8. Results of cyclic triaxial test on loose sand (after Seed and Lee, 1966).

Effect of soil density

The previous discussion pertains to the behavior of sands with low relative density. The response of sand to cyclic loading is very much dependent on the relative density of the sand. DeAlba et al. (1976) showed the number of cycles necessary to induce the 100 percent pore pressure ratio condition is strongly influenced by the relative density of the soil. The general relationship is shown in Figure 9.

In addition to being more resistant to pore water pressure increases, dense sands also exhibit a quite different behavior after the 100 percent pore pressure ratio state has been achieved. Unlike the loose sand, when a dense sand is subjected to shear strain there is an initial contraction followed by dilation as the strain increases. The resulting
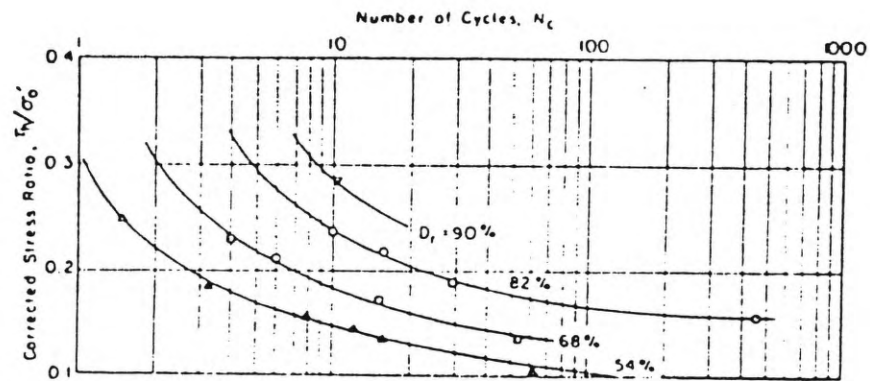
Figure 9. Stress ratio versus number of cycles necessary to
cause liquefaction (after DeAlba et al., 1976).

sequence of events is as follows: 1) the sand densifies until the 100 percent pore
pressure ratio state is reached, 2) the sand begins to strain and as a consequence
dilates, and 3) as a result of dilation, the pore water pressure drops and the effective
stress returns to a non-zero value. In this manner the sand regains its shear resistance
after a limited amount of strain.

Seed and Lee (1966) also ran cyclic triaxial tests on dense sands (Figure 10).
Comparison of Figure 10 with Figure 8 illustrates the great difference in behavior
between dense and loose sands.
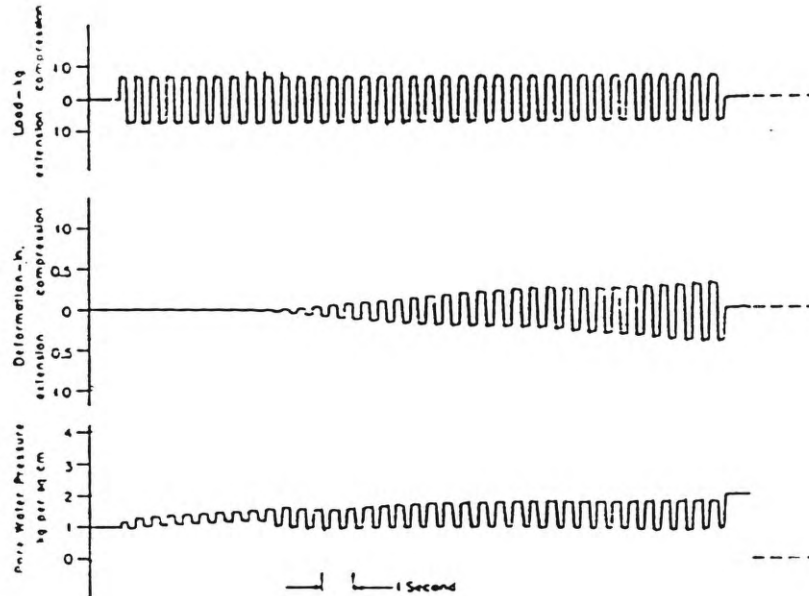
Figure 10. Results of cyclic triaxial test on dense sand (after Seed and Lee, 1966).

Shear strength after cyclic loading

The behavior of soils following cyclic loading is important since it is the residual strength that greatly affects the failure of the soil. After a sufficient amount of straining the soil reaches a constant steady-state of deformation where the steady-state shear strength of the soil is only a function of void ratio and is independent of stress history (NRC, 1985). Figure 11 demonstrates this phenomena with stress strain curves for a monotonically loaded dense sand (Figure 11a) and an identical sample that was cyclically loaded followed by monotonically loaded (Figure 11b). It can be seen that the steady-state shear strength, s_{us}, is the same in both cases.

Figure 12 shows the results of the same type of tests as in Figure 11 on a loose
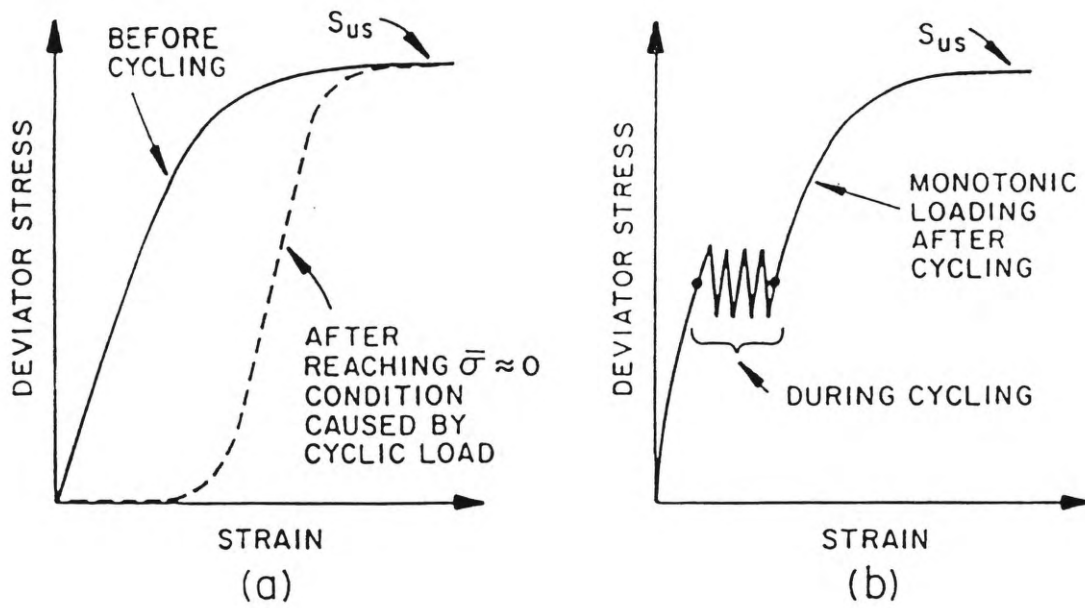
Figure 11. Stress versus strain diagram for monotomically and cyclically loaded samples of dense sand (after NRC, 1985).
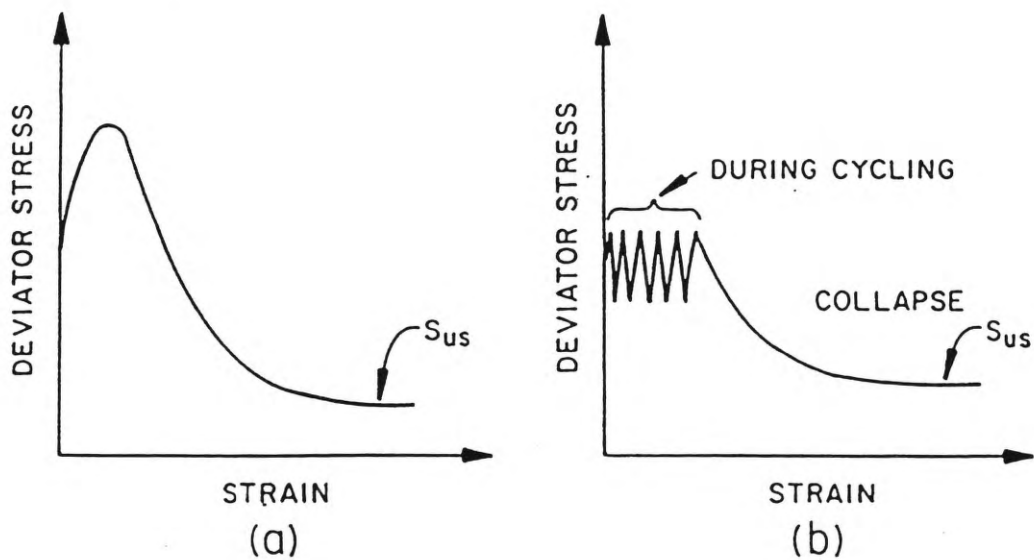
Figure 12. Stress versus strain diagram for monotomically and cyclically loaded samples of loose sand (after NRC, 1985).

sand. The steady-state shear strength of the cyclically loaded sample is actually slightly higher than the monotonically loaded sample (due to a lower void ratio as a result of cyclic loading). However, the peak shear strength experienced by the monotonically loaded sample was never experienced by the cyclically loaded sample. Thus, in the monotonically loaded sample, the shear strength will never be lowered to the steady-state deformation value as long as the stress stays below the peak shear strength and the soil does not experience cyclic loading.

Castro and Poulos (1977) resolved that the behavior of the dense sand in Figure 11b is not true liquefaction but rather should be called cyclic mobility. Cyclic mobility refers to the process where a soil undergoes deformation during cyclic loading due to pore water pressure buildup but then regains its strength when the cyclic loading has ceased. On the other hand, the soil behavior illustrated in Figure 12b is true liquefaction. The soil has lost its strength and will continue to strain until the shear stress has become very small.

The preceding discussion further illustrates the importance of soil density in the development of liquefaction.

Upward flow of water

After cyclic stresses have ceased and the soil has consolidated, the excess pore water pressure needs to dissipate. The result is an upward flow of water into overlying

soil layers. If the gradient of the upward flow of water into overlying soil is great enough to cause a "quick" condition the overlying soils will essentially liquefy. The result is an upward propagation of liquefied soils that would otherwise have been stable (Seed, 1979).

Failure Mechanisms

The manifestation of liquefied soils on the ground surface or in relation to a structure can usually be grouped into one of three catugories: 1) lateral spreads, 2) flow failures and 3) loss of bearing capacity (Youd, 1978; Youd, 1973; NRC, 1985). The slope of the ground greatly influences the type of failure mode. Lateral spread failures generally occur on gentle slopes, usually between 0.5 and 5 percent grade, where as flow failures usually occur on slopes greater than 5 percent (Youd, 1978). Bearing capacity failures can occur on any degree of slope but, since lateral spreads and flow failures tend to dominate on slopes, they are more commonly the failure mechanism on level ground. Bearing capacity failures are often the result of upward migration of pore water (Seed, 1979; Seed and Idriss, 1967; Youd, 1978).

Lateral spreads

Lateral spreads are the lateral movement of surface soils as a result of liquefaction and deformation of subsurface layers. Lateral displacements are on the order of several

feet and have been reported at several tens of feet in highly susceptible regions (Seed and Idriss, 1967; Grantz et al., 1964).

Damage from lateral spreads can range from the rupture of buried pipes to the collapse of structures due to differential settlement of the foundation. Often bridges are severely disrupted when the flood-plains move toward the river channel causing compression of the bridge (Figure 13)(Youd, 1978).

Flow failures

Flow failures are the most violent of failures attributed to liquefaction. Flows can move many tens of feet at speeds of many tens of miles per hour (Youd, 1978). The flow can consist of a completely liquefied mass or contain blocks of intact material riding in and on the liquefied soil.
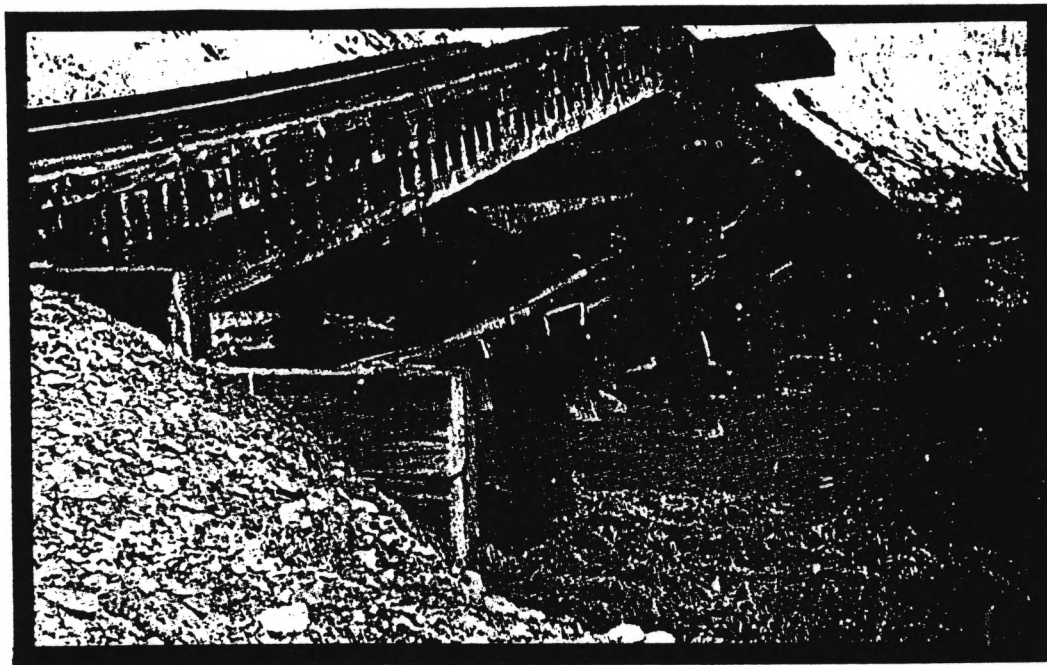
Figure 13. Bridge compressed and buckled by lateral spreading during the 1964 Anchorage Earthquake (after NRC, 1985).

Bearing capacity failures

Bearing capacity failures occur when a structure or its foundation loses support when the bearing material liquefies. These failures can be manifested as subsidence and rotation of buildings or as the rising of buried and pipes due to buoyant forces. Figures 14 and 15 show bearing capacity failures in the form of tilting buildings and buoyant tanks.

Other failure mechanisms

Several other failure mechanisms have been observed that do not distinctly fall under one of the above mentioned groups. A brief discussion of each of these mechanisms follows.

Sand boils. Sand boils occur when a mixture of soil particles and water travels upward to the surface through cracks and fissures from a zone of excess pore water pressure. This excess pore water pressure is often the result of the liquefaction phenomena. When the soil-water mixture reaches the ground surface the soil is deposited in cone shaped piles or ridges in the case of long fissures. Often sand boils occur in the time period shortly following the earthquake since it takes time for the pore water pressure to reach the surface. Although sand boils rarely cause serious damage, they can cause damage to pavements and superficial building damage (NRC, 1985).

Ground oscillations. Ground oscillations (also referred to as lurching) occur when a relatively intact soil layer overlies a liquefied layer. The intact layer will break into blocks

Figure 14. Tilting of apartment buildings during the 1964 Niigata earthquake (after Seed and Idriss, 1967).

Figure 15. Sewage treatment tank floated to ground surface during 1964 Niigata earthquake (after Seed and Idriss, 1967).

that oscillate on the liquefied soil. Often this is observed as ground waves on the surface (NRC, 1985).

Ground settlement. Ground settlement occurs as a result of the soil structure densification during cyclic straining. Settlements can be on the order of up to five feet as observed in the 1964 Anchorage Earthquake (Grantz et al., 1964). Damages attributed to ground settlements are due to differential settlements under structures of flooding due to the ground subsiding below the water table.

Methods of Analyzing Liquefaction Susceptibility

Liquefaction susceptibility, opportunity and potential.

Liquefaction potential is a probabilistic measure of the likelihood of liquefaction occurring. The potential in this study will be expressed as a probability of occurring in a 100 year period. Liquefaction potential can be broken down into two components; liquefaction opportunity and liquefaction susceptibility.

Liquefaction opportunity is a function of the seismicity of the region. It is expressed as a probability of a site experiencing ground motions of intensity large enough to cause liquefaction. It has nothing to do with the soil characteristics.

Liquefaction susceptibility, on the other hand, is a measure of the stresses (or strains) necessary to cause liquefaction. It is a function of the soil and site characteristics. Liquefaction susceptibility is expressed as a minimum measure of cyclic

strain required to cause liquefaction. These minimum measures will be discussed in the following sections.

Once parameters for liquefaction susceptibility and opportunity have been determined, the liquefaction potential of a site or area can be determined by finding the probability of minimum cyclic strain (the susceptibility) being exceeded in the time period of interest (the opportunity). The evaluation of liquefaction susceptibility is discussed in this section. Liquefaction potential will be discussed in the sections dealing with liquefaction mapping techniques. Although liquefaction opportunity values, in the form of exceedence probability curves, will be used to determine liquefaction potential, their development is not in the scope of this thesis and they will be discussed only briefly in the methodology section.

Factors affecting liquefaction susceptibility

Liquefaction susceptibility of a soil has been identified to be a function of several factors dealing with properties of the soil and its environment. These properties are (Seed, 1979; Seed and Idriss, 1971, 1982):

Soil Properties
1. Dynamic shear modulus
2. Damping characteristics
3. Unit weight
4. Grain size and shape
5. Relative Density
6. Soil structure

Environmental Properties
1. Method of soil formation (depositional environment)
2. Seismic history
3. Geologic history (aging, cementation)
4. Lateral earth pressure coefficient
5. Depth to water table
6. Effective confining pressure

Although the influence of all these factors cannot be measured directly, their effects

should be considered in any susceptibility analyzing method.

Simplified procedure

Representative stresses. Seed and Idriss (1971) derived a relationship for the

average value of cyclic shear stress developed during an earthquake. The equation:

$$\tau_{av} \approx 0.65 \cdot (\gamma \cdot h/g) \cdot a_{max} \cdot r_d \qquad (1)$$

approximates the average cyclic shear stress, τ_{av}, at any depth, h, where γ is the unit

weight of the soil, g is the acceleration of gravity and r_d is a correction factor to account

for the fact that the soil column is not a rigid body. Figure 16 shows the range of values

of r_d for different soil profiles. One should note that for depths less than 40 feet, the

range of r_d values is small and using the average value will generally involve an error of

less than five percent.

The coefficient value of 0.65 is included to reduce the value of maximum shear

stress, τ_{max}, to a value of average shear stress, τ_{av}. Figure 17 shows a typical time

history of shear stress during a hypothetical earthquake. After taking the weighted

$$r_d = \frac{\left(\tau_{max}\right)_d}{\left(\tau_{max}\right)_r}$$
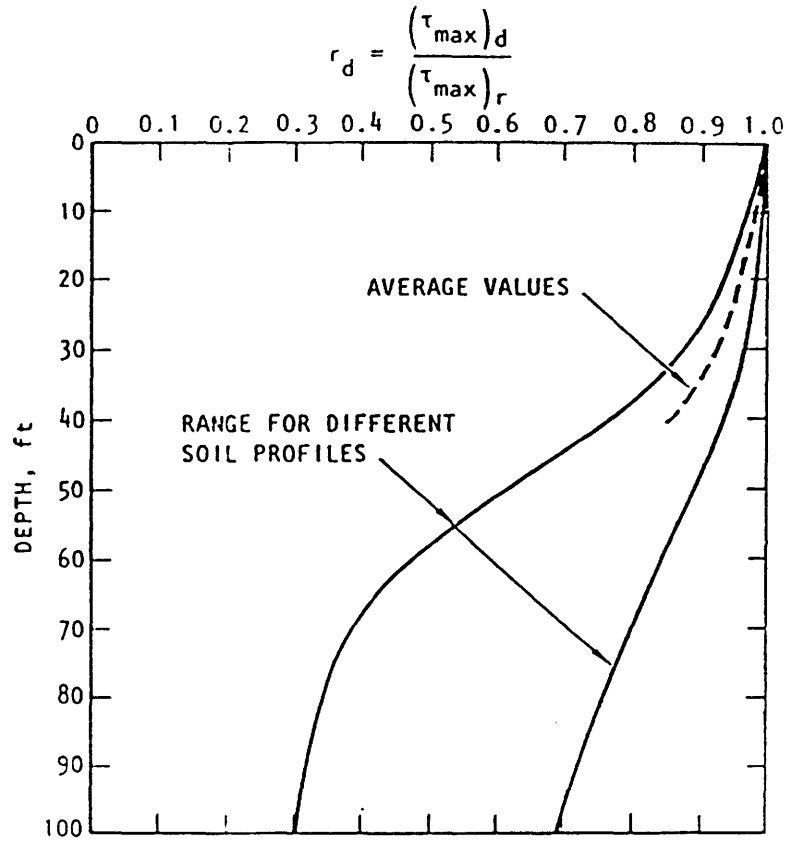
Figure 16. Range of values or r_d (after Seed and Idriss, 1982).
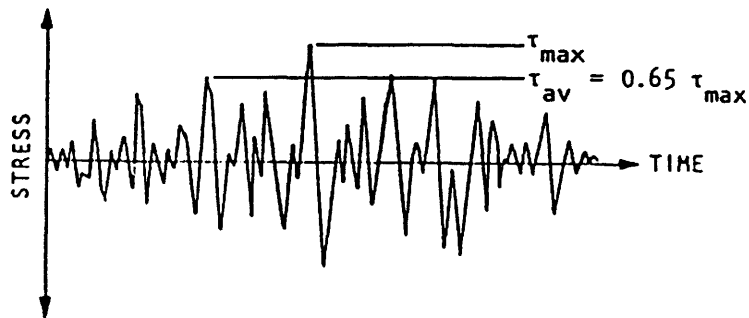
Figure 17. Time history of shear stress during earthquake (after Seed and Idriss, 1982).

average values of shear stress from several earthquake records like Figure 17, Seed and

Idriss (1971) concluded that τ_{av} is usually about 65 percent of τ_{max}.

Table 1 gives representative values of the number of equivalent stress cycles, N_c,

experienced for a given magnitude of earthquake. Using the value of τ_{av}, from Equation

1, and the value of N_c, from Table 1, yields a simple way of evaluating the stresses

induced on a soil during an earthquake. Laboratory testing can then be used to

determine the behavior of the soil during the earthquake.

Table 1. Number of representative cycles for various earthquake magnitudes (after Seed and Idriss, 1982).

Earthquake Magnitude	No. of Significant Stress Cycles, N_c
5.25	2-3
6.0	5
6.75	10
7.5	15
8.5	26

Laboratory testing. Cyclic simple shear tests and cyclic triaxial tests have been

used to try and model the effects of earthquake ground motions on soils (Seed and

Peacock, 1971). DeAlba et al. (1976) later modeled earthquake motions using

multidirectional shear tests conducted on a shaking table, which are more representative

of actual earthquake motions. The tests indicated that the stress values determined from

cyclic simple shear tests should be reduced by about 10 percent to provide results representative of multidirectional stress conditions. Likewise, it was determined that triaxial test data should be corrected using the equation:

$$\tau_h/\sigma_v' \approx C_r \cdot (\sigma_{dc}/2 \cdot \sigma_a)_{tri}$$ (2)

where C_r values are approximately:

$C_r = 0.57$ for $K_o = 0.4$
$C_r = 0.9$ to 1   for $K_o = 1$

and

τ_h/σ_v' is the ratio of the cyclic shear stress to the effective overburden stress causing liquefaction in multidirectional shear tests (cyclic stress ratio), σ_{dc} is the cyclic deviator stress and σ_a is the ambient confining pressure (Seed and Idriss, 1982).

Although laboratory tests seem to be a viable procedure for determining liquefaction susceptibility several inherent difficulties have been recognized. These include (Seed and Idriss, 1982):

1. Acquisition of undisturbed samples
2. Selection of representative samples
3. Avoidance of stress concentrations during testing.

While these difficulties can be overcome or compensated for, nevertheless, they do make laboratory testing a costly and involved process.

Analysis based on SPT data

It has been noted that the major factors affecting the cyclic stress ratio of a soil

also affect the blow counts of the Standard Penetration Test (SPT) in the same manner. Table 2 summarizes these factors and their effects on liquefaction and standard penetration resistance. With this in mind, it was hypothesized that the SPT would be a good means of assessing the liquefaction susceptibility of soils (Seed, 1979).

Table 2. Factors affecting soil liquefaction characteristics and penetration resistance.

Factor	Effect on stress ratio required to cause liquefaction	Effect on penetration resistance
Increased relative density	Increases stress ratio for liquefaction	Increases resistance
Increased stability of structure	Increases stress ratio for liquefaction	Increases resistance
Increase in time under pressure	Increases stress ratio for liquefaction	Probably increases resistance
Increase in K_o	Increases stress ratio for liquefaction	Increases resistance
Prior seismic strains	Increases stress ratio for liquefaction	Probably increases resistance

After the Niigata Earthquake of 1964 work started correlating SPT data to the value of induced cyclic stress ratio required to cause liquefaction. Since then, after

additional research has been conducted and much more data collected, a procedure has been refined into a reliable basis for determining liquefaction susceptibility (Seed and Idriss, 1982).

Standard Penetration Test. The SPT test is conducted by driving a standard sampling tube into the soil by dropping a 140 pound hammer 30 inches onto the drill rods. The standard penetration resistance, N, is the number of blows required to drive the sampler one foot into the ground. Despite its name, the SPT test is not always consistent due to differences in hammer dropping technique, drilling methods and sampler size.

Seed et al. (1985) recognized these sources of variability in proposing a truly standard procedure as well as correction procedures for nonstandard results. The standard procedure proposed by Seed calls for a hammer dropping mechanism that delivers 60 percent of the energy of the dropping hammer to the drill rods, a borehole four to five inches in diameter, a drill bit that deflects drilling mud upward, a standard split spoon sampler (O.D.=2.00 in.; I.D.=1.38 in.), A or AW drill rods, 30-40 blows per minute and N values measured over the range from 6-18 inches of penetration.

The hammer efficiency of 60 percent is characteristic of a safety hammer raised and dropped using a one inch rope wrapped twice around a pulley. For techniques having different hammer efficiencies the equation:

$$N_{60} = N_m \cdot (ER_m/60) \tag{3}$$

N_{60} = N at 60% efficiency

N_m = N at m% efficiency

can be used to correct the N values to the standard value. Other factors must be corrected by producing empirical relationships between the standard and nonstandard procedures.

Interpreting SPT data. Seed et al. (1983) developed a procedure for evaluating liquefaction susceptibility using a modified value of the standard penetration resistance. The basic procedure uses a normalized penetration resistance, N_1, representative of the penetration resistance at one ton per square foot. If the soil is silty, a correction factor is added to N_1. The value of N_1 is then compared to an empirically developed relationship and a value of the cyclic stress ratio required to induce liquefaction is determined.

The standard penetration resistance, N, is influenced by the effective confining pressure at the depth where the test was performed. Since depth is already considered in the cyclic stress equation (Equation 1), it is desirable to eliminate the effect of confining pressure from the SPT analysis. This is done using a normalized value of the penetration resistance, N_1. N_1 is calculated from the relationship:

$$N_1 = C_N \cdot N \tag{4}$$

where C_N is an empirical function relating the penetration resistance at the depth of the test to penetration resistance where effective confining pressure is equal to one ton per square foot. Values of C_N can be obtained from Figure 18 after the effective confining pressure at the test depth has been calculated (Seed and Idriss, 1982).

It is now necessary to correlate between the cyclic stress ratio needed to cause liquefaction and normalized penetration resistance. Seed et al. (1977) plotted N_1 against cyclic stress ratio known, or estimated, to have occurred during a magnitude 7.5 earthquake. This data is shown on Figure 19. Locations that experienced liquefaction are indicated on the plot. From this data, a lower bound, below which liquefaction is not expected to occur, can be determined. Figure 19 provides an empirical means of converting a value of N_1 into a minimum value of cyclic stress ratio required to cause liquefaction during a magnitude 7.5 earthquake.

As was previously stated, the number of cycles of stress a soil is subjected to greatly effects the magnitude of the stress required to induce liquefaction. Figure 20 shows this general relationship. Using the number of stress cycles inflicted by an earthquake of given magnitude (Table 1), the ratio of the value of cyclic stress ratio needed to induce liquefaction during that earthquake to the like value for a 7.5 earthquake can be calculated from data read from Figure 20. Using these ratios, curves resembling the curve for a magnitude 7.5 earthquake in Figure 18 can be plotted for different magnitudes. These curves are plotted on Figure 21. Using Figure 21 one can
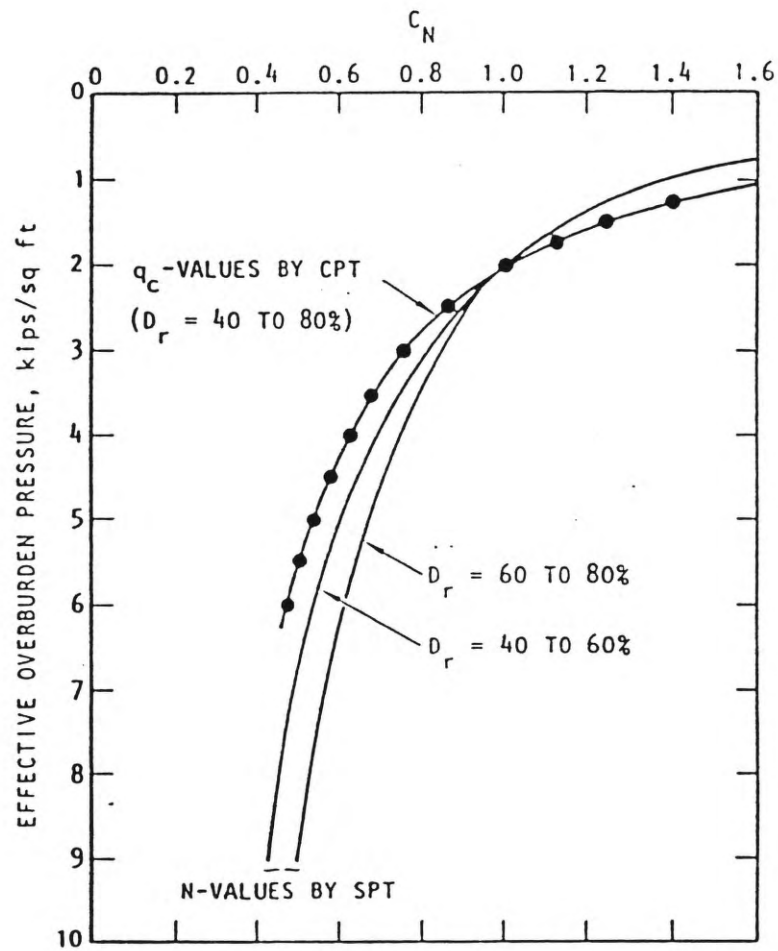
Figure 18. Chart for values of C_N (after Seed and Idriss, 1982).

42
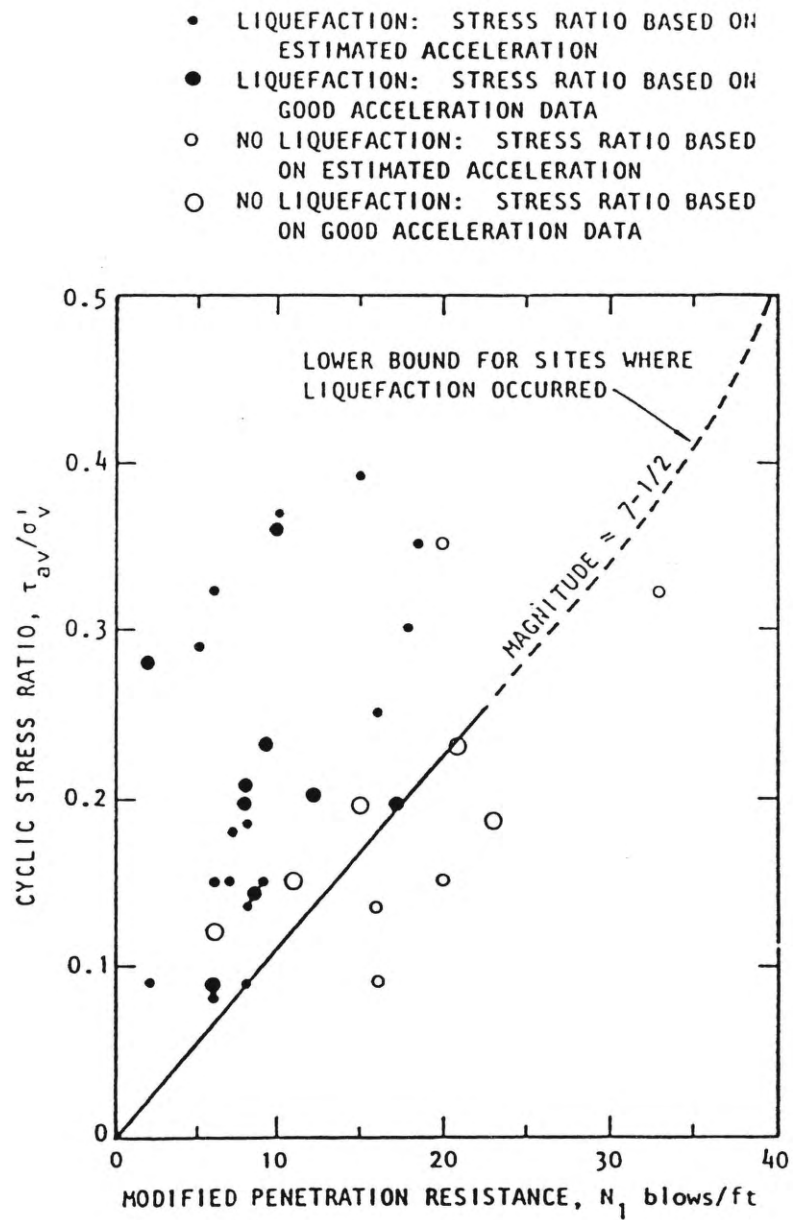
Figure 19. Correlation between cyclic stress ratio required to cause liquefaction and normalized penetration resistance of sand (after Seed et al., 1977).

now find the cyclic stress ratio required to cause liquefaction for different earthquake
magnitudes.
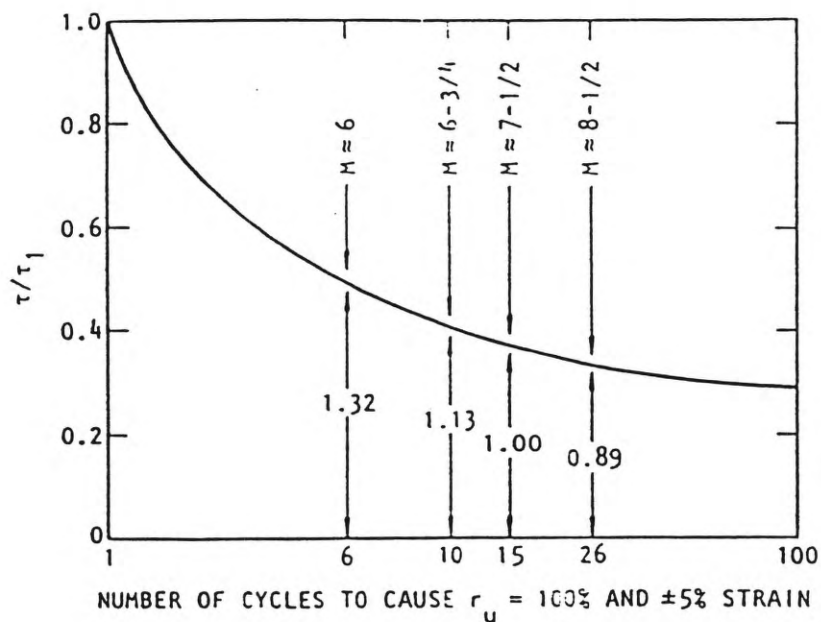
Figure 20. Relationship between shear stress and number of cycles required to
cause liquefaction. Ratios of required shear stress to correlate between
different earthquake magnitudes are shown (after Seed and Idriss, 1982).
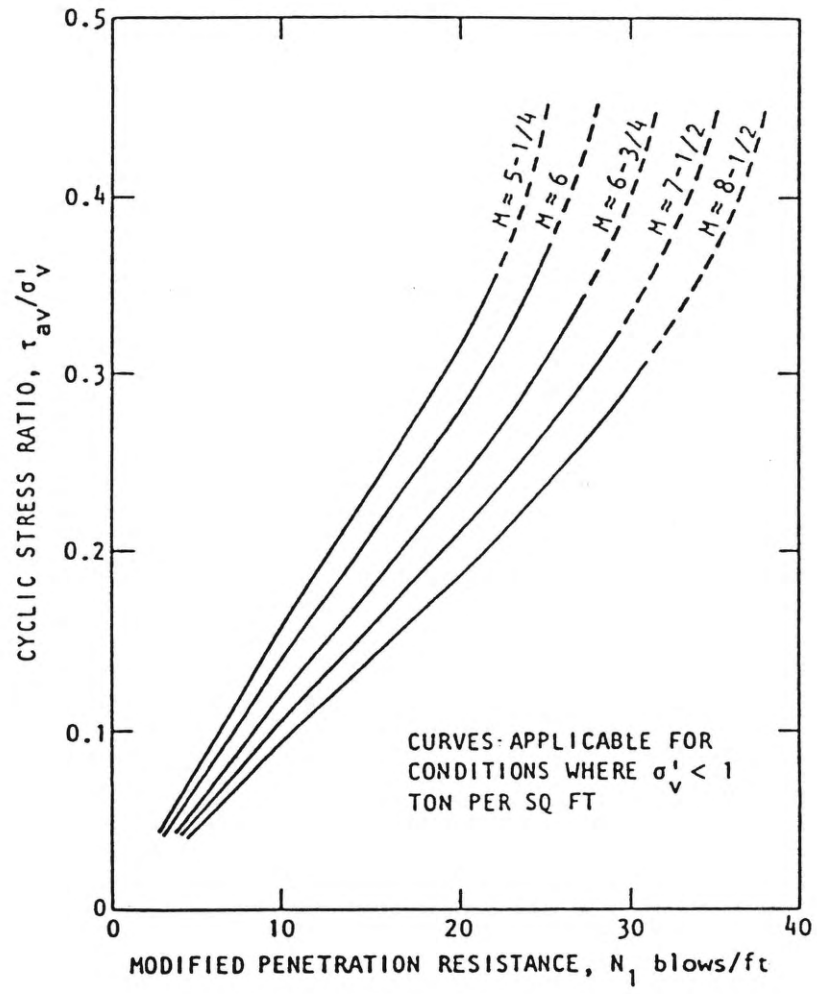
Figure 21. Chart to correlate cyclic stress ratio required to cause liquefaction with normalized penetrtion resistance for different magnitude earthquakes (after Seed and Idriss, 1982).

The preceding discussion and Figure 21 are applicable to clean sands only. If a soil contains an appreciable amount of fine material it will have a greater resistance to liquefaction due to the cohesive effect of the fines. When a graph similar to Figure 19 is produced for silty sands (D_{50} < 0.15mm) a boundary line separating soils experiencing liquefaction from the nonsusceptible soils can be drawn (Figure 22). Note that this line is essentially parallel to the line for clean sands (D_{50} > 0.25mm). Furthermore, it can be determined that N_1 for silty soils is essentially equal to that of clean sands plus 7.5. Therefore, a modified penetration resistance is calculated by adding 7.5 to the normalized penetration resistance for silty soils. this modified penetration resistance is then used in conjunction with the appropriate curve on Figure 21 to determine the cyclic stress ratio required to induce liquefaction.

The method described above is the most widely used liquefaction susceptibility analyzing technique and is the technique used in this study.

Analysis using cone penetration data

The cone penetration test. The cone penetration test (CPT) is performed by pushing an electronic cone (Figure 23) (or mechanical cone in older models) into the ground, at a constant rate, and recording the bearing resistance against the tip (Q_c), and friction resistance against the friction sleeve (F_s). Empirical correlations have been
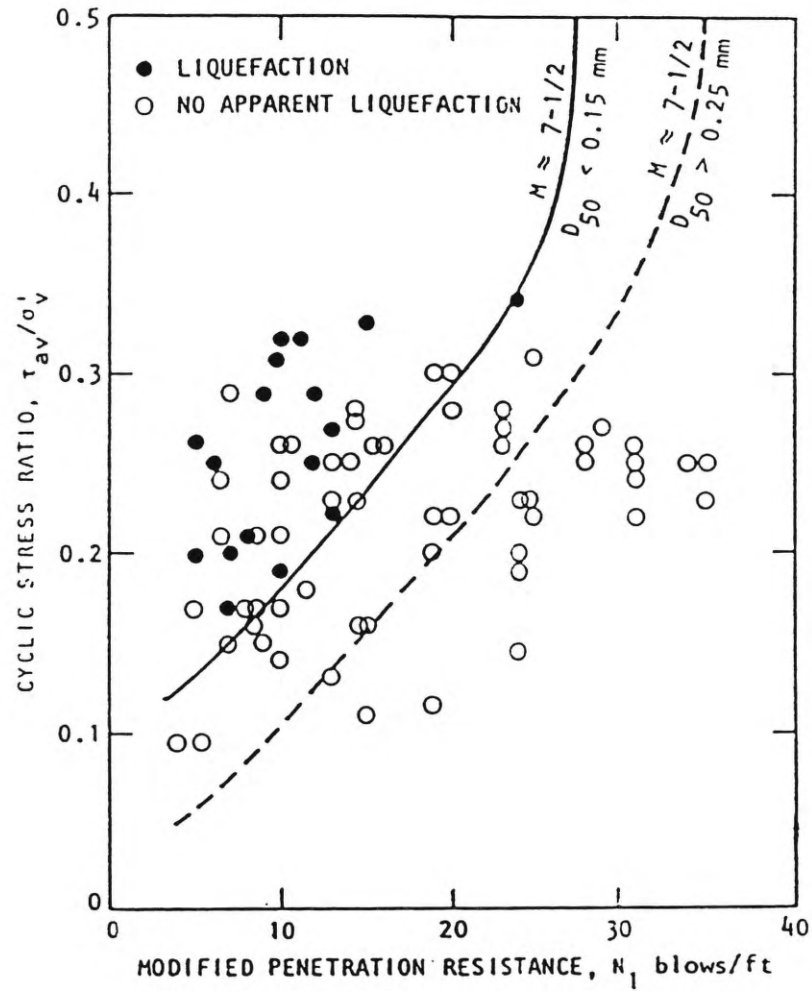
Figure 22. Correlation between silty sands and clean sands for field liquefaction behavior during a magnitude 7.5 earthquake (after Seed and Idriss, 1982).
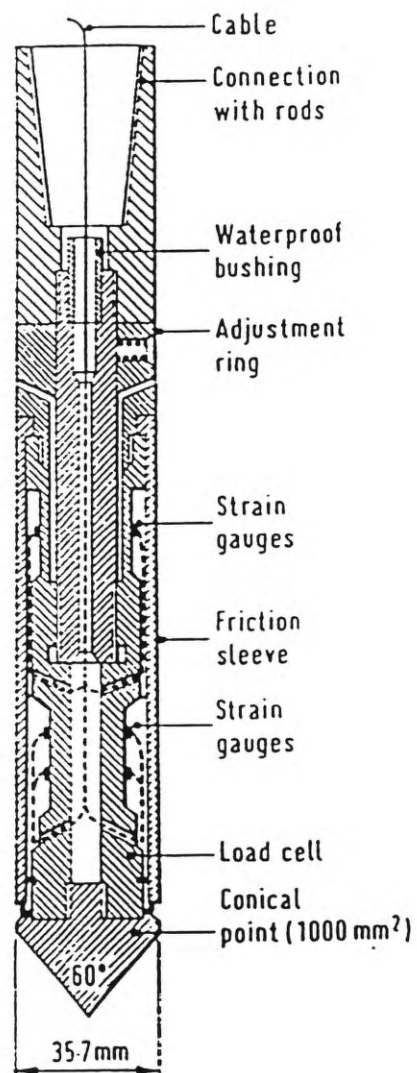
Figure 23. Electronic cone penetrometer (after Meigh, 1987).

developed to convert the data obtained from the CPT test into usable data such as soil type and properties. Often CPT data is correlated with SPT data so that the vast amounts of research dealing with SPT data can be used to interpret the results.

Liquefaction susceptibility analysis. Generally, liquefaction susceptibility analysis is determined from CPT data by first converting it into soil type and equivalent standard penetration resistance, N. Once this has been done, the same procedure that was used with the SPT test can be used to determine liquefaction susceptibility (Seed et al., 1983).

Correlation of CPT data to soil type is achieved by plotting the friction ratio (F_r, the ratio of the friction resistance to the tip resistance) verses the log of the tip resistance. One of the several relationships that have been developed from this technique is shown in Figure 24. Variations in these types of plots are due in a large part to the differences in the depositional environments of the soils that were used for the data. Therefore, it is always necessary to correlate or adjust the soil classification chart for every different study area (Robertson and Campanella, 1986).

The correlation between CPT data and SPT data is a linear relationship between the tip resistance, Q_c, and the standard penetration resistance, N. Schmertmann (1977) determined that for clean sands Q_c is usually in the range of 4.0 to 5.0 times N and for silty sands Q_c usually ranges between 3.5 to 4.5 times N. As was necessary with the soil classification, preliminary studies should be conducted in each new area to establish a
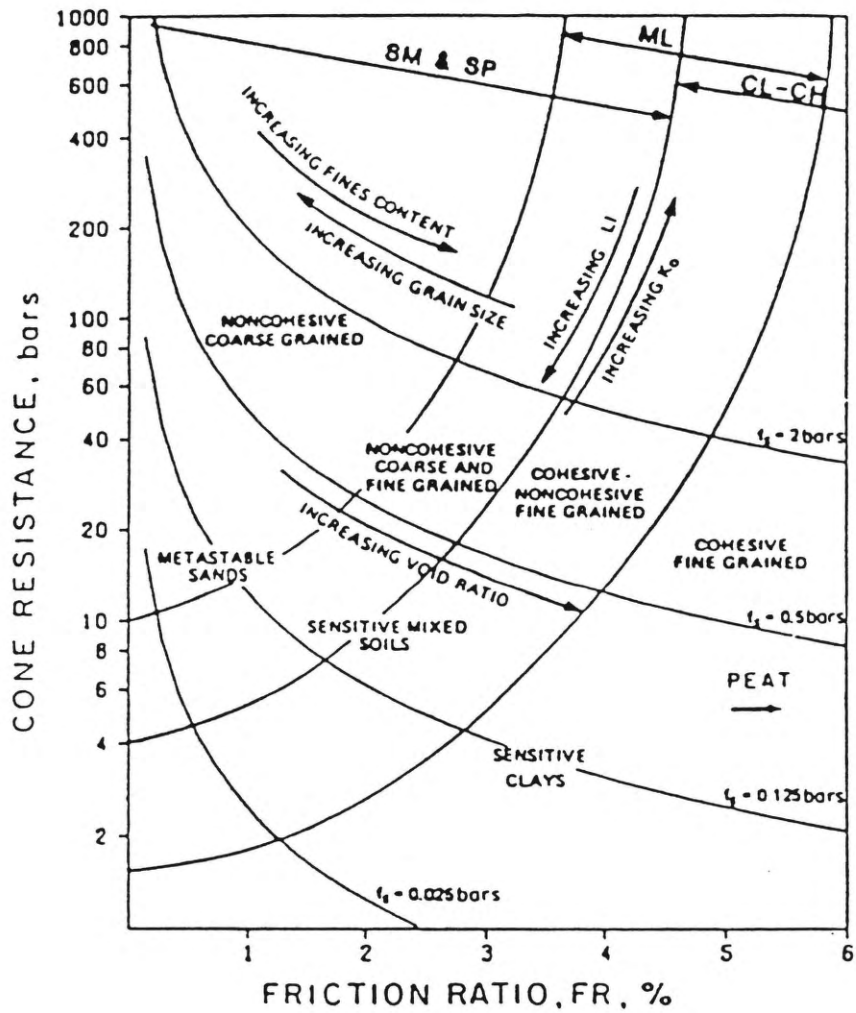
Figure 24. Soil classification chart for cone penetrometer (after Douglas and Olsen, 1981).

good correlation with the soils in the area.

Threshold strain method. As mentioned previously, the rate at which soils tend to consolidate is strongly influenced by the magnitude of cyclic strain that is experienced by the soil. With this in mind, it would make sense to evaluate liquefaction susceptibility on the basis of strains experienced by a soil rather than the stresses applied. A method which estimates shear strain by measuring shear wave velocity through soil shows promise of becoming a reliable and relatively easy to apply method of analysis.

The maximum strain experienced in a soil during an earthquake can be estimated with the equation (NRC, 1985):

$$\gamma = \tau/G = ((a/g) \cdot \sigma_o \cdot r_d)/G \tag{5}$$

γ = Maximum shear strain
τ = Maximum shear stress
G = Shear modulus of the soil
a = Maximum ground acceleration
g = Acceleration of gravity
σ_o = Total vertical stress
r_d = Stress reduction factor (Figure 16).

If it assumed that the unit weight of the soil is uniform with depth, Equation 5 reduces

to: $$\gamma = (a \cdot z \cdot r_d)/((G/GG_{max})_\gamma \cdot V_s^2) \tag{6}$$

z = depth
$(G/G_{max})_\gamma$ = modulus reduction factor for strain

Generally, $(G/G_{max})_\gamma$ can be estimated as 0.8 and the equation reduces to:

$$\gamma = (1.2 \cdot a \cdot z)/V_s^2 \tag{7}$$

The threshold strain, below which no soil densification can occur, can now be estimated at any depth as a function of the peak acceleration and shear wave velocity.

Dobrey et al. (1987) rearranged Equation 7 to solve for acceleration and plotted the acceleration necessary to reach the threshold strain value. Figure 25 shows a sample of the results of this procedure. Assuming a value of threshold strain, one can now estimate a critical acceleration required to start soil densification from shear wave velocity. Since initial densification is indicative only of the first step of the liquefaction process, this procedure tends to be very conservative when used to evaluate liquefaction susceptibility. Nevertheless, with more research currently being conducted, the method shows much promise of becoming a popular susceptibility analysis technique.
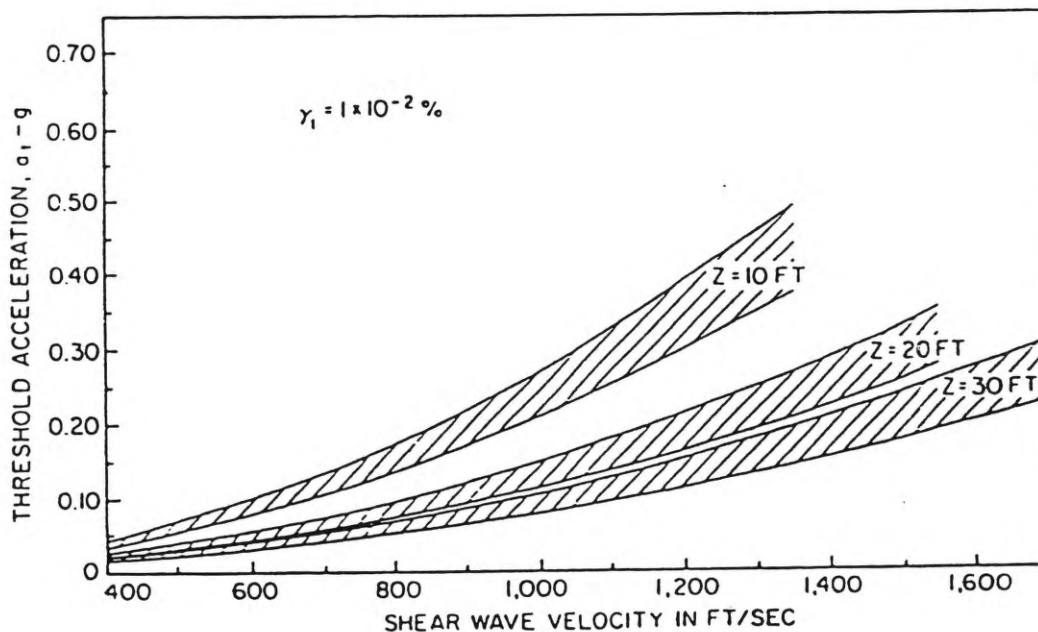
Figure 25. Critical acceleration prediction chart for threshold strain of 0.01% (after Dobrey et al., 1981).

Mapping the Liquefaction Hazard

In the past decade several procedures have been used to identify the areas where soils susceptible to liquefaction exist. Although the methods varied between the procedures, the same basic scheme of analysis was used throughout. This basic scheme consists of comparing the liquefaction susceptibility of the soils with the opportunity of the site experiencing ground motion to determine some measure of the liquefaction potential. The analysis has ranges from qualitative procedures such as mapping on geologic criteria to more quantitative approaches such as the probabilistic methods to be discussed in a later section.

Mapping based on geologic criteria

Influence of geology on liquefaction susceptibility. As mentioned earlier, there are numerous properties of the soil and its surrounding environment that affect the liquefaction susceptibility of an area. Sedimentary deposits can also be classified as having a number of these properties. Therefore, one can assume that certain types of sedimentary deposits will be more susceptible to liquefaction than others.

Youd and Perkins(1978),while working in California,evaluated the effects of these properties on the liquefaction susceptibility of these deposits.The age of the deposit as well as the type of deposit was considered in determining the likelihood that these deposits contain liquefiable soils.A summary of these evaluations is presented in Table

3.

Youd and Perkins (1978) then developed a procedure for mapping liquefaction potential using the data of Table 3. The first step of the procedure is to construct a liquefaction susceptibility map by identifying the sedimentary deposits and assigning them estimates of susceptibility based on Table 3. Then a liquefaction opportunity map is produced by analyzing the seismicity and the ground motion attenuation relationships for the region. Finally a liquefaction potential map is produced by superimposing the previous two maps (Youd and Perkins, 1978).

Tinsley et al. (1985) used the basic procedure of Youd and Perkins in mapping liquefaction potential in the Los Angeles region, however, they used subsurface geotechnical data to supplement the geologic data. After mapping the sedimentary units, the thickness of the units were determined from borehole data. The liquefaction susceptibility for each borehole was then calculated for earthquake magnitudes of 6.5 and 8.5 and groundwater levels at the surface and at depths of 10 and 30 feet using the method of Seed et al. (1983). Those areas that were susceptible to liquefaction during a magnitude 6.5 earthquake were classified as having high liquefaction potential while those found nonliquefiable during a magnitude 8.5 earthquake were classified as having low liquefaction potential. Results of these tests were in good general agreement with Table 3 and, therefore, supported the conclusions of Youd and Perkins well.

Table 3. Estimated susceptibility of sedimentary deposites to liquefaction during strong seismic shaking
(after Youd and Perkins, 1978).

Type of Deposit	General distribution of cohesionless sedements in deposito	Likelihood that cohesionless sediments, when saturated, would be susceptible to lique- faction (by age of deposit)			
		< 500 Yr.	Holocene	Pleistocene	Pre-pleistocene
Continental deposites					
River Channel	Locally variable	Very high	High	Low	Very Low
Flood-plain	Locally variable	High	Moderato	Low	Very Low
Alluvial fan and plain	Widospread	Moderato	Low	Low	Vory Low
Marin terraces ahd plains	Widespread	_	Low	Very Low	Very Low
Delta and fan delta	Widespread	High	Moderate	Low	Very Low
Lacustrine and playa	Variable	High	Moderate	Low	Very Low
Colluvium	Variable	High	Moderate	Low	Very Low
Talus	Widespread	Low	Low	Very Low	Very Low
Dunes	Widespread	High	Moderate	Low	Very Low
Loess	Variable	High	High	High	Unknown
Glacial Till	Variable	Low	Low	Very Low	Very Low
Tuff	Rare	Low	Low	Very Low	Very Low
Tephra	Widespread	High	High	?	?
Residual Soils	Rare	Low	Low	Very Low	Very Low
Sebka	Locally variable	High	Moderate	Low	Very Low
Costal Zone					
Delta	Widespread	Very high	High	Low ·	Very Low
Esturine	Locally variable	High	Moderate	Low	Very Low
Beach					
High wave energy	Widespread	Moderato	Low	Very Low	Very Low
Low wave energy	Widespread	High	Moderate	Low	Very Low
Lagoonal	Locally variable	High	Moderate	Low	Very Low
Fore shore	Locally variable	High	Moderate·	Low	Very Low

It should be noted that Table 3 is valid for the California area only and that in other areas environmental and geologic conditions could cause major variations in the behavior of soils. For example, in mapping liquefaction potential along the Wasatch Front in Utah, Anderson and Keaton (1982) found a considerable amount of the Lake Pleistocene Lake Bonneville deposits to be potentially liquefiable. The fact that a large amount of these deposits are liquefiable shows Figure 3 to be invalid in this area. Thus, in order for this technique to be applicable, a region specific study of the characteristics of sedimentary deposits must be conducted.

Probabilistic methods of analysis

Liquefaction probability. A probabilistic measure of liquefaction potential can be evaluated by comparing the conditional probability of liquefaction (liquefaction susceptibility) to the expected intensity of seismic loading (liquefaction opportunity). Kavazanjian et al. (1985) expressed the probability of liquefaction with the equation:

$$P[L] = \int_i P[L/i] \, f_i(i) \, di \tag{8}$$

P[L]   = Probability of liquefaction
P[L/i] = Conditional probability of liquefaction given an occurrence of seismic loading intensity
$f_i(i)$ = Probability density function of intensity level i

The conditional probability of liquefaction expresses the probability of liquefaction given a particular level of seismic loading intensity. The probability density function of intensity can be evaluated in terms of earthquake recurrence and ground motion attenuation

relationships. The function is usually expressed in terms of an acceleration exceedence

probability curve which plots annual probability of occurrence versus the maximum

acceleration.

San Francisco, California. Kavazanjian et al. (1985) mapped liquefaction potential

in San Francisco using the basic probabilistic technique described above. The first step

of their analysis was to determine a design RMS (Root Mean Squared) acceleration (r_a)

from the exceedence probability curve based on a chosen level of recurrence. Then the

RMS cyclic shear stress ratio required to cause liquefaction (r_s') was calculated from the

equation:

$$r_s' = f\, r_a\, \sigma_o/\sigma_o' \qquad\qquad (9)$$

f = flexibility factor (Equivalent to r_d of Seed and Idriss (1971)
σ_o = total vertical stress
σ_o'= effective vertical stress

This equation is very similar to the equation of Seed and Idriss (Equation 1). The soil

characteristics are accounted for by empirically determining the density ratio (D_r) from

the SPT data. To determine the conditional probability of liquefaction, lab tests were

conducted to relate D_r, the number of cycles required to induce liquefaction and r_s'. An

analysis, outlined by Chameau and Clough (1983), that weighs the effects of different

numbers of cycles based on the recurrence probabilities of different magnitude

earthquakes, was then used to determine the conditional probability of liquefaction given

a value of RMS acceleration. Thus, by knowing the relative density of the soil and the

RMS acceleration expected in the time period of interest, the probability of liquefaction occurring during the designated time period can be computed.

Wasatch Front, Utah. Anderson and Keaton (1982) developed a probabilistic procedure for mapping liquefaction potential along the Wasatch Front in Utah. This method uses SPT data and the liquefaction susceptibility analysis procedure of Seed et al. (1983) to compute the cyclic stress ratio required to cause liquefaction. With the value of cyclic stress ratio known, Equation 1 can be rearranged to solve for the critical acceleration required to cause liquefaction, $(a_{max})_c$:

$$(a_{max})_c = (\tau_{av}/\sigma_o') \cdot (\sigma_o'/\sigma_o) \cdot (1/0.65r_d) \tag{10}$$

The value of $(a_{max})_c$ can then be compared to a exceedence probability curve to determine the probability of it being exceeded.

In mapping liquefaction potential Anderson and Keaton (1982) calculated the accelerations that had a 50, 10 and 5 percent chance of being exceeded in a 100 year period. The critical accelerations for each boring were then plotted on the map and contours drawn along the acceleration values mentioned above. Liquefaction potential was then classified as high for areas with critical accelerations having a probability of exceedence of over 50 percent in 100 years, moderate for probability between 10 and 50 percent, low for probability between 5 and 10 percent and very low for probability less than 5 percent. The contour lines were later adjusted to follow along the geologic contacts which form the natural boundaries between the probability zones.

Liquefaction severity index

The mapping techniques previously described only delineate zones where soils are likely to undergo pore pressure increases that lead to the zero effective stress condition. However, Youd and Perkins (1987) pointed out that the liquefaction hazard is not only a function of the soils likelihood to liquefy, but that other factors come into play that affect the severity of damage that occurs. These factors include: seismologic, topographic, sedimentologic, hydrologic and engineering properties of the deposit. In order to more effectively map the liquefaction hazard Youd and Perkins (1987) developed the parameters of liquefaction severity (S) and liquefaction severity index (LSI).

After studying many case histories, Youd and Perkins (1987) came to the general conclusion that little damage occurs to structures when differential displacements are less than two to four inches. Likewise, the conclusion was made that major damage is likely to occur when displacements are of 30 inches or more. To quantify these observations, the parameter of liquefaction severity is defined as the differential displacement due to liquefaction in inches.

Since severe damage is likely to occur when the S-value is equal to 100 or more a second parameter, LSI, is introduced. LSI is defined as the maximum S-value for lateral spreads on wide active flood-plains, deltas or other areas of gently slopping late Holocene fluvial deposits. By defining LSI in this way the parameter is normalized with

respect to all the previously mentioned factors except seismicity. The value of LSI ranges from 0 to 100 with areas having S-values greater than 100 being assigned the limiting value of 100.

Since LSI is normalized with respect to all factors except seismicity, LSI can be described in terms of ground motion characteristics. Specifically, Youd and Perkins described ground motion in terms of earthquake magnitude (M) and the logarithm of the distance from the seismic source (R) or, in equation form:

$$LSI = f(M, Log\ R) \tag{11}$$

To evaluate this relationship, known LSI values were evaluated for earthquakes covering a wide range of magnitudes throughout the western United States. To this data Youd and Perkins applied a linear least squares analysis which produced the equation:

$$Log(LSI) = -3.49 - 1.86(Log\ R) + 0.98\ M \tag{12}$$

where R is the horizontal distance from the seismic event in kilometers. It should be noted that Equation 10 was derived for the western United States and is not applicable in other regions.

Youd and Perkins used Equation 12 and the seismologic information to map LSI in the San Diego, California region.

Utilizing Liquefaction Potential Maps

Liquefaction potential maps define zones in which liquefaction has a certain probability of occurring. Liquefaction is not expected to occur at every site in a zone when the region experiences ground motion intensities exceeding the specified critical accelerations of the zone; however, it could be assumed that damage due to liquefaction will be confined to zones corresponding to the ground motion intensity experienced.

Table 4 is a matrix developed by Anderson and others (1987) for determining the required site specific investigation for various types of structures in different liquefaction potential zones. Use of this matrix will help planners and developers to determine when an investigation into the liquefaction susceptibility of a site is appropriate and necessary.

It is important to realize that liquefaction is one of a number of geologic hazards that could affect a site. In order to effectively mitigate the hazards, one must start with an understanding of which hazards exist and how each hazard contributes to the risk. The hazards can then be dealt with in a way that effectively reduces the total risk from all risk components.

Table 4. Required site specific investigation for liquefaction
potential zones (after Anderson et al., 1987).

Facility	Liquefaction Potential Zone			
	High	Moderate	Low	Very Low
CRITICAL Hospital Fire Stàtion Police Station Other emergency facilities	YES	YES	YES	MAYBE
LIFELINES Communications Transportation Water Supply Electricity Natural Gas Sewage Plants	YES	YES	YES	MAYBE
HIGH OCCUPANCY PUBLIC OWNED Schools State Capitol City Hall County Courts Airports Sports/Convention Cntr.	YES	YES	YES	MAYBE
HIGH OCCUPANCY PRIVATE OWNED Offices Apartments Shopping Malls Hotels	YES	YES	YES	MAYBE
INDUSTRIAL SEVERE CONSEQUENCE Refineries Sewage Plants Hazard/Toxic Explosive	YES	YES	MAYBE	NO
INDUSTRIAL MINOR CONSEQUENCE Trucking Shipping Light Manufacturing	NO*	NO*	NO	NO
RESIDENTIAL SUBDIVISION	MAYBE*	NO*	NO	NO
RESIDENTIAL SINGLE LOTS	NO*	NO*	NO	NO

*Appropriate Disclosure Required

METHODOLOGY

General Overview of Mapping Process

In this study, the mapping of liquefaction potential was performed following the general method of Anderson and Keaton (1982). However, due to the extreme scarcity of existing subsurface data and limited funds available to conduct a supplementary field investigation, the interpretation techniques had to be modified in order to more effectively interpolate between the data points that were available. This was accomplished by using the Quaternary geology of the area to define zone boundaries while the subsurface data was used to define the soil properties within these zones.

The mapping process can be divided into three steps: 1) collection of data, 2) analysis of data and 3) interpretation of results of the analysis in the form of liquefaction potential maps. Subsurface data was collected from a number of local engineering firms and state agencies. Geology and ground water reports were also obtained mainly from the United States Geological Survey. After all existing data was collected a supplementary investigation was planned and conducted to supply information in areas previously not investigated. The data was then analyzed to produce a numerical probability of liquefaction occurring in a 100 year period. The results of the analysis were plotted on a base map so that zones depicting liquefaction potential of the areas could be delineated.

Collection of Existing Data

Boring logs, test pit logs and laboratory soil test results were collected from a number of local engineering firms as well as the Utah Department of Transportation and the Utah State Engineer's office. Although SPT results, or some other similar form of penetration test, are necessary to compute critical accelerations, data from test pits is also useful for insight into the general nature of deposits. Geology and ground water reports were available for most of the study area that gave a general small-scale interpretation of the Quaternary geology and groundwater conditions of the areas.

Supplementary Field Investigation

In areas where little or no subsurface data existed, a supplementary field investigation was conducted. The investigation consisted of three shallow borings performed with a hand operated drill rig, 13 borings performed with a CME 50 drill rig mounted on an all-terrain vehicle and 23 electronic cone penetrometer soundings. Additional cone penetrometer soundings were attempted in the Park City-Heber area but it was not possible to penetrate more than a few feet into the gravelly deposits.

The purpose of the borings performed with the hand operated rig was to provide inexpensive data on subsurface and ground water conditions in regions not expected

to be liquefiable. Hand operated borings could not be drilled to depths much greater than 25 feet, thus limiting their usefulness. Borings performed with the drill rig were conducted at sites where cone soundings were conducted. The purpose of these borings was to establish a region specific correlation between CPT data and SPT and soil data.

The borings were performed using continuous flight augers. Samples were taken using a two foot long split spoon sample at four foot intervals. A constant head of water was maintained in the augers to prevent a quick condition which would effect the results of the SPT tests. Figure 26 shows a typical log of one of the borings performed for this study.

The cone soundings were performed using the data retrieval system designed by Bay (1987) and used in the Northern Utah liquefaction mapping project. The system uses a Campbell Scientific 21X micrologger to read the tip and friction resistance every half inch of depth. The values recorded by the micrologger are dumped to a cassette tape which can then be down-loaded to a microcomputer. The data points were then averaged over six inches and plotted as shown in Figure 27.

Much care was taken in planning the supplementary field investigation in order to optimize the effectiveness of the limited number of sites that could be analyzed. The investigation was limited to the Juab, Sevier and Sanpete Valleys and the Park City-Heber area. This was done for two reasons: first, these areas contained the highest

65
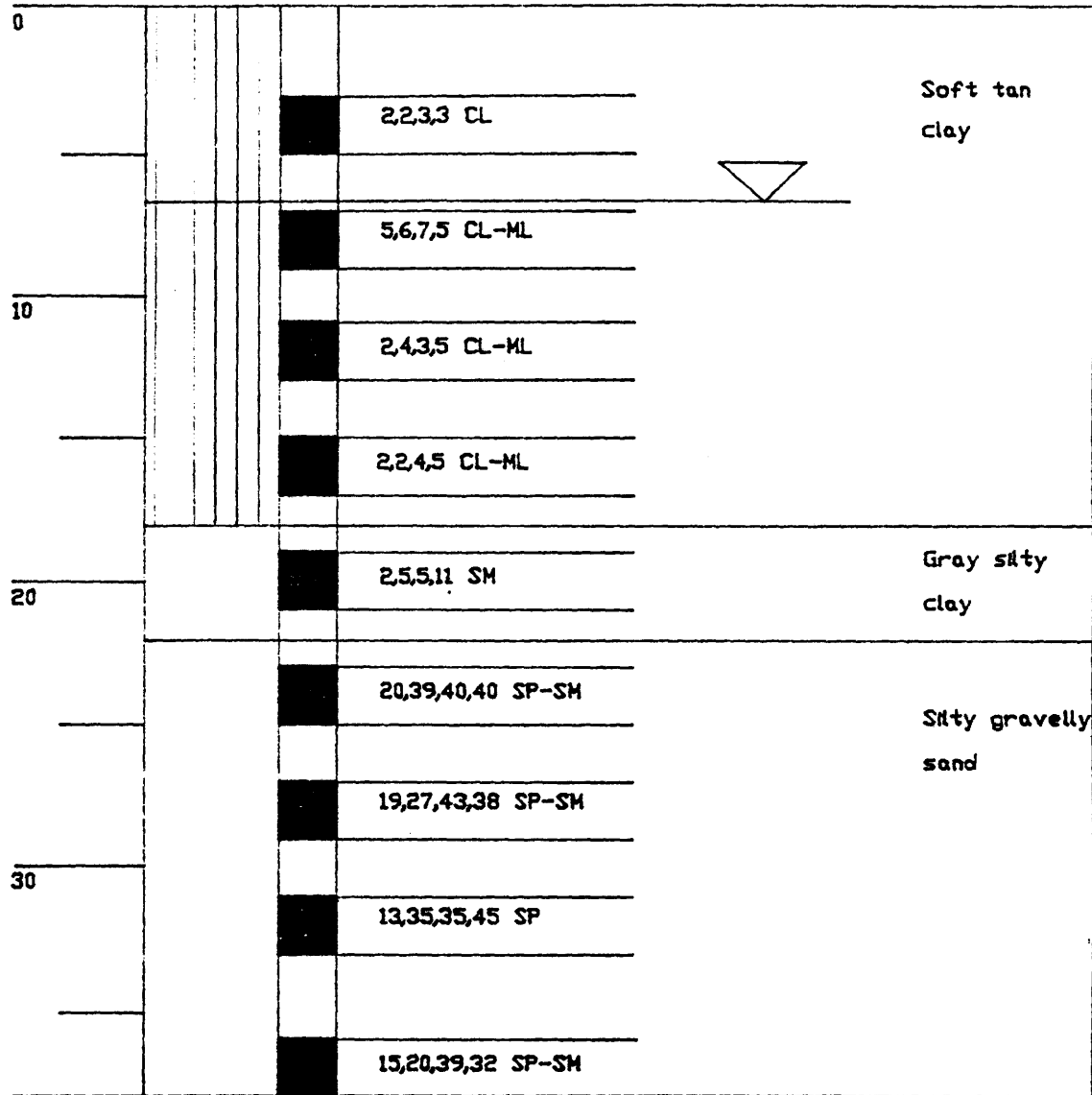
Figure 26. Example of boring log from field investigation.
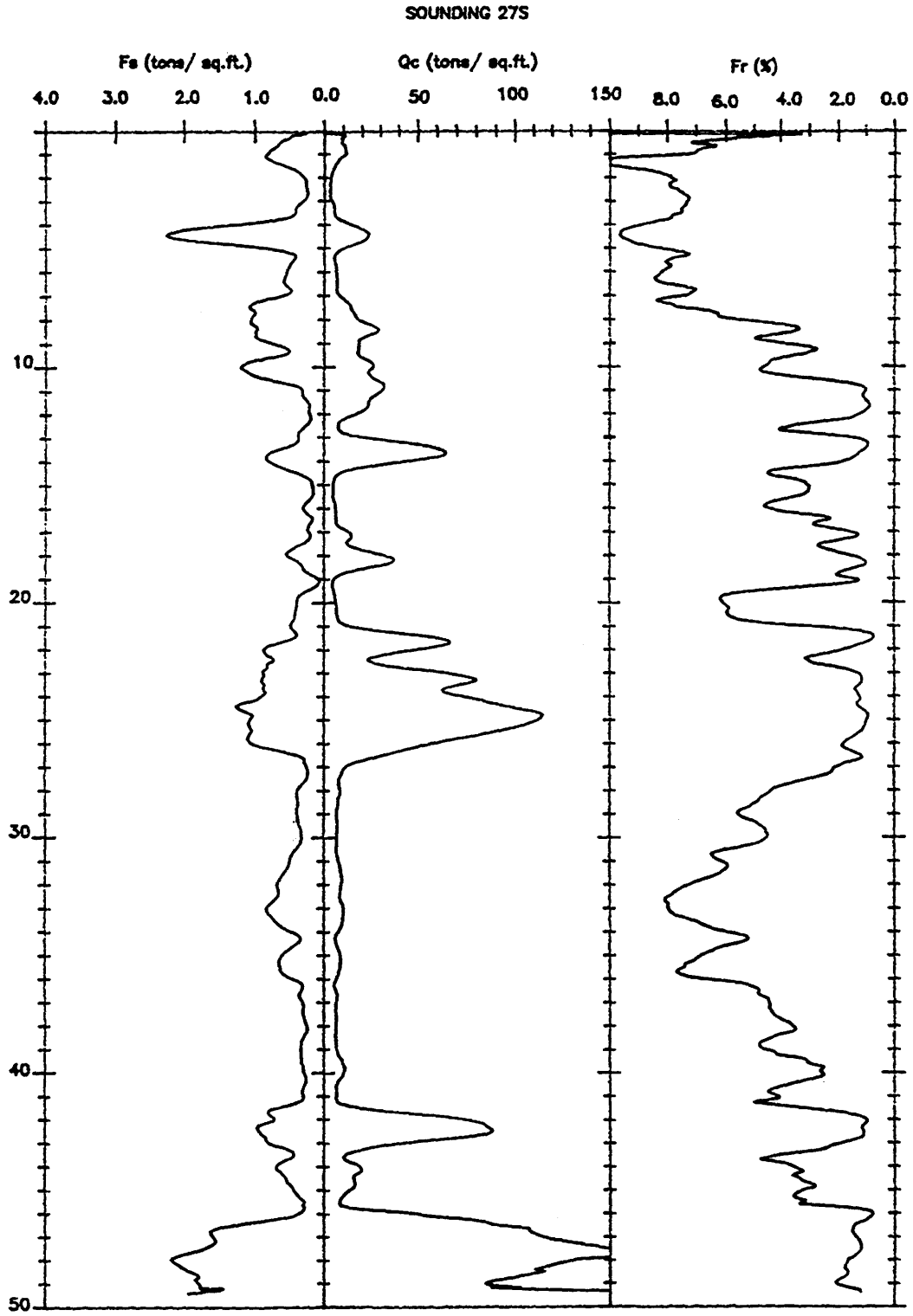
SOUNDING 27S

Figure 27. Example of cone sounding from field investigation.

density of population and development and, secondly, these deposits were less laterally continuous than in the Sevier Desert and Pavant Valley regions.

In the Sevier Desert region, because of the nonhomogeneous nature of the Lake Bonneville-Sevier River deposits (see geology section), it was concluded that addition of any supplementary borings would not significantly increase our understanding of subsurface conditions. The existing data and surficial geology suggest that the subsurface consists of discontinuous beds of sand interbedded with clay and silt. Additional borings could locate and analyze some of these sand beds but would not be useful in establishing general subsurface trends across the region as was possible in other regions of the study. Thus, it was decided to classify the area according the existing data and to use surficial geology to delineate lateral changes in subsurface conditions.

Determining Critical Accelerations

Critical accelerations values were calculated using the computer programs CRAC and CRACCO written by Jim Bay (1987) that were modified for use in this study on an IBM compatible micro computer. Modifications generally involved input and output operations. Calculating routines were generally not changed except for minor computer language differences. In addition to modifications required for IBM compatibility

modifications of constant parameters were necessary to account for different seismic conditions and cone penetrometer-soil correlations. The modified programs were renamed PCCRAC and PCRACCO.

Critical accelerations from SPT data

Creating data files. A program called BORIN was written to create data files for input into PCCRAC. BORIN is an interactive program that assembles soil, ground water and SPT data into an input file. The program also handles some nonstandard penetration test data encountered in the study that PCCRAC has been programmed to convert to SPT data. After the input file has been created it can be edited in a program editor. After editing, the program REORG is used to transform the input file from sequential access to direct access as required for PCCRAC.

Input files can contain as many borings as desired. The only limitation is that all boring areas must have the same earthquake magnitude.

Calculating critical accelerations. The program PCCRAC uses the method of Seed et al. (1983) to calculate the cyclic stress ratio required to cause liquefaction. The critical acceleration required to cause liquefaction is then calculated using Equation 8. All of the empirical relationships used in the analysis are evaluated in the program using a polynomial fitted to the curve of the representative graph using a least squares analysis.

Input required to run PCCRAC includes the data file compiled by BORIN and

REORG and the design earthquake magnitude. PCCRAC calculates a critical acceleration for every penetration test conducted in a liquefiable soil. The output lists critical acceleration, cyclic stress ratio, the depth of the test and the soil type.

Critical accelerations from CPT data

Regional correlation of data. The first step in calculating critical accelerations from cone penetration data is to convert CPT data into soil type and equivalent standard penetration resistance (N). In order to do this, a region-specific correlation study must be conducted. This was accomplished by comparing the data of SPT tests conducted in the supplementary investigation with data of the adjacent CPT test. The data from this study was compared to that of Bay (1987) and found to be compatible. Therefore, both sets of data were combined and used for the correlation. Combining data produced a larger data base so that calculations can be made with more accuracy.

The soil type correlation was performed by plotting friction ratio (F_r) versus the logarithm of tip resistance (Q_c) and distinguishing between soil types being plotted. Figure 28 shows the results of the combined data plotted in this fashion. The data for this study was divided into three soil types: 1) clean sands, 2) silty sands and silts and 3) clays. The boundaries separating these soil types are shown in Figure 28. These soil

SOIL CLASSIFICATION CHART
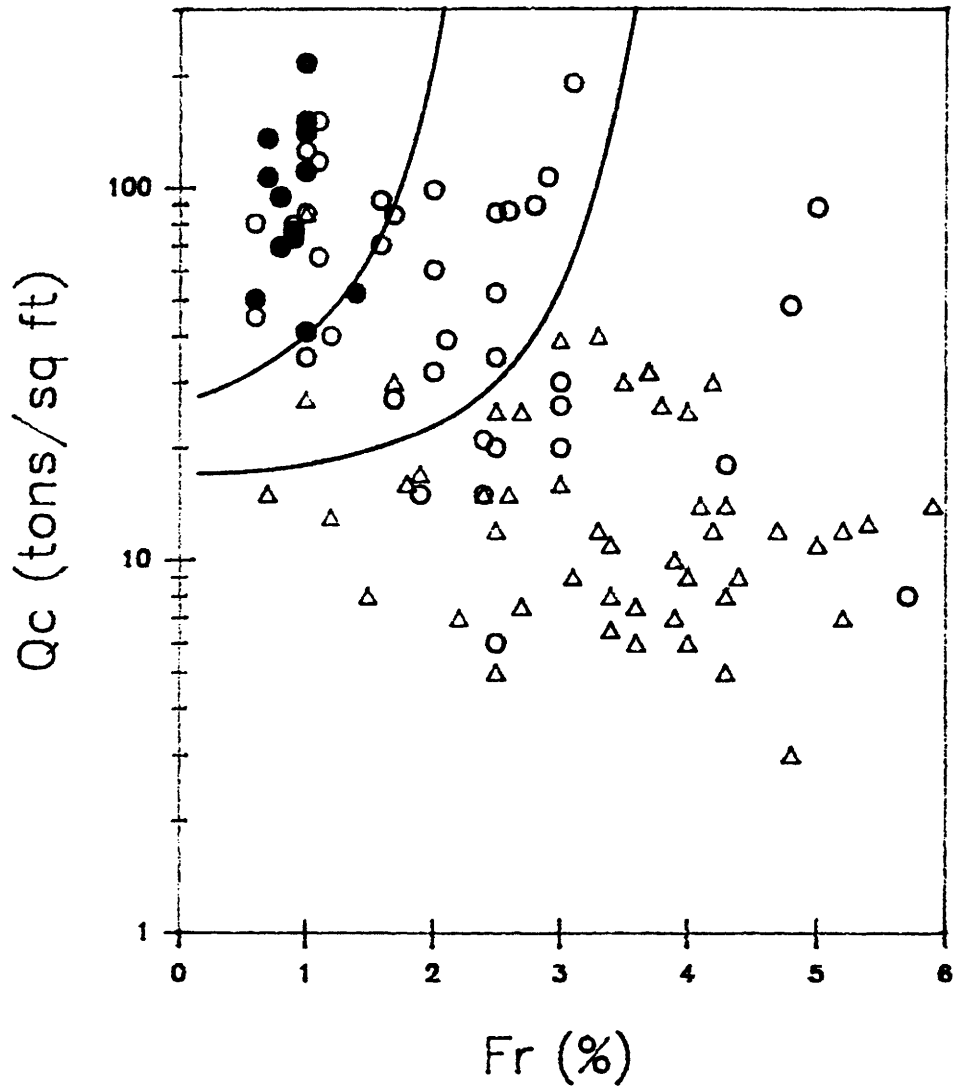
Figure 28. Soil classification chart for CPT data, generated from field investigation data.

types were chosen for two reasons: 1) the soils could be distinguished with a reasonable degree of accuracy and 2) the soils correlate well with the silt correction and the liquefaction behavior of different soil types. For clean sands no silt correction was used while for silty sands and silts a correction of 7.5 was used. Clays were not considered to be liquefiable.

The boundaries of Figure 28 are plotted on a soil classification chart proposed by Robertson (1985) (Figure 29). It can be seen that the boundaries coincide fairly well with this chart. However, comparison with other published soil classification charts, such as Figure 24, does not produce as good agreement. This further emphasizes the need for a region specific correlation.

To correlate between CPT data and N, the ratio of Q_c/N was determined for the two liquefiable soil types. Figure 30 shows a plot of N versus Q_c for clean sands. From the slope of the line, it can be seen that Q_c/N is about equal to 4.6. Figure 31 shows the same plot for silty sands and silts. In this case Q_c/N was found to equal about 3.35.

The values of Q_c/N determined for this study agree well with those determined previously by Robertson (1985) and Schmertmann (1977). For clean sands both Robertson and Schmertmann arrived at values of Q_c/N from 4.0 to 5.0. While for silty sands Schmertmann found Q_c/N values between 3.5 and 4.5, where as Robertson determined boundary values of 3.0 and 4.0. Again, the results of this study agree well with those of Robertson as they did with his soil classification chart.
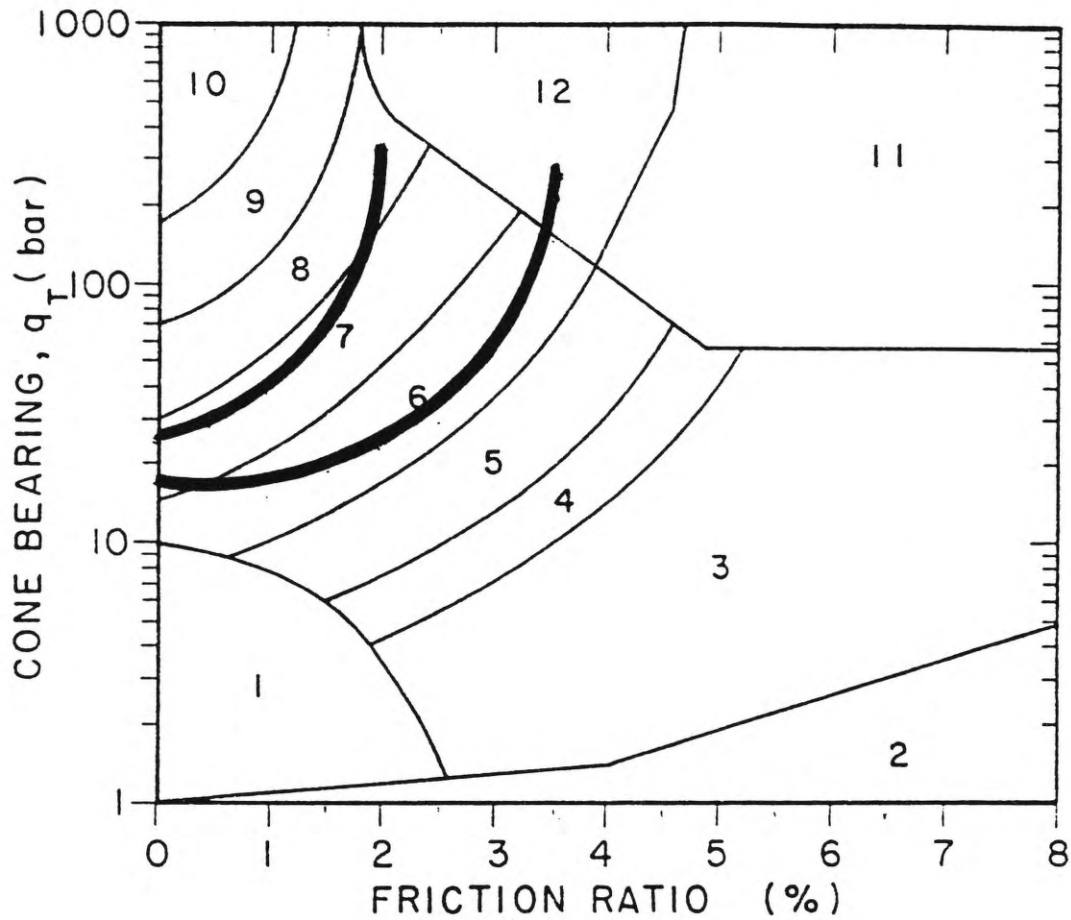
Zone	Qc/N	Soil Behaviour Type
1)	2	sensitive fine grained
2)	1	organic material
3)	1	clay
4)	1.5	silty clay to clay
5)	2	clayey silt to silty clay
6)	2.5	sandy silt to clayey silt
7)	3	silty sand to sandy silt
8)	4	sand to silty sand
9)	5	sand
10)	6	gravelly sand to sand
11)	1	very stiff fine grained (*)
12)	2	sand to clayey sand (*)

(*) overconsolidated or cemented

Figure 29. Comparison of soil classification curves from field investigation data with soil classification chart of Robertson (1985).
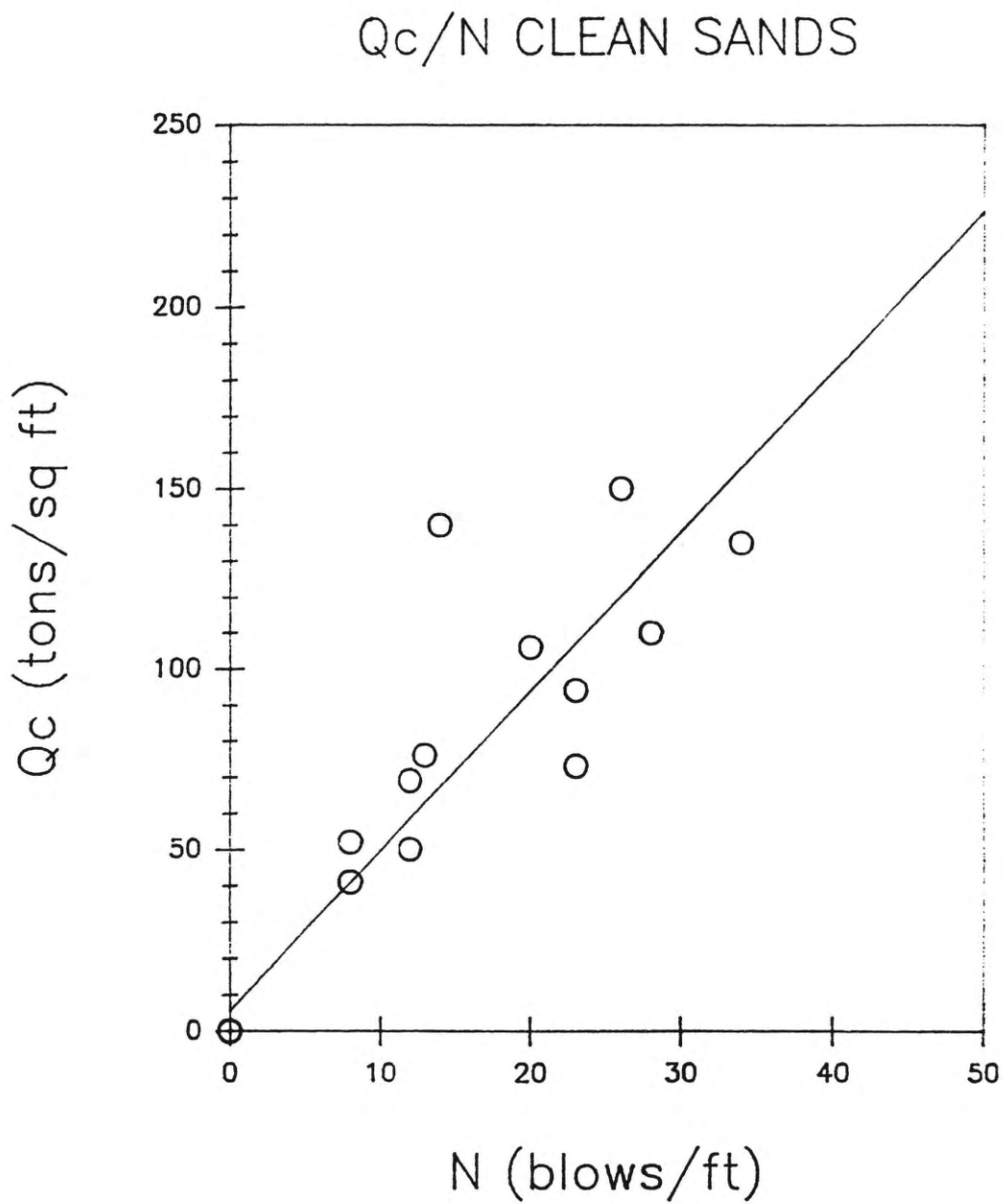
Figure 30. Qc/N correlation for clean sands.
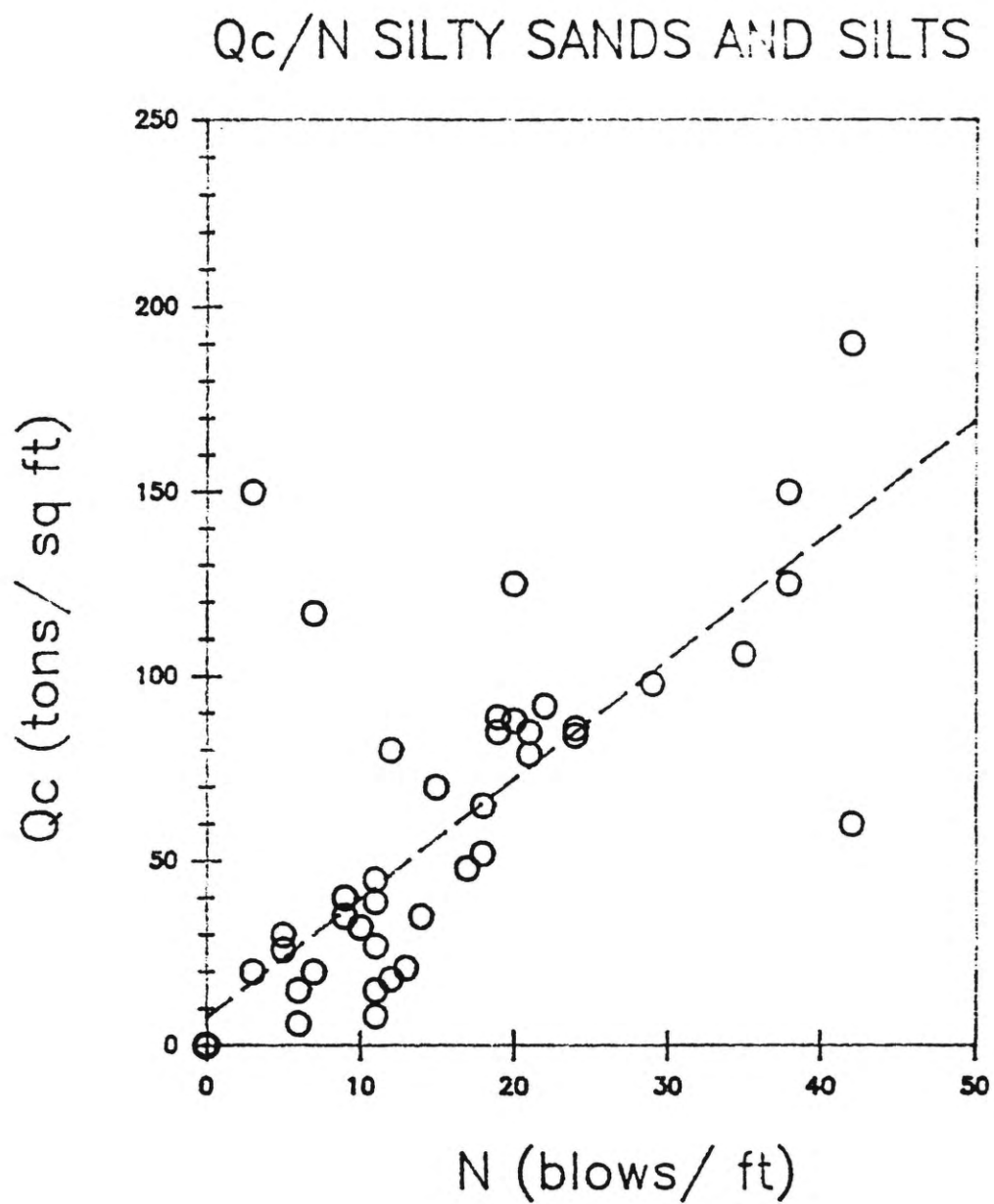
Figure 31. Qc/N correlation for silty sands and silts.

Calculating critical accelerations. The program PCRACCO was used to calculate critical accelerations from CPT data.In the first step of the analysis, the program converts the CPT data into equivalent soil type and standard penetration resistance. PCRACCO then uses the same routines as PCCRAC to calculate the critical acceleration for every data point (every 1/2 inch). A data file is produced that contains depths and critical accelerations for clean sands and silty sands. This data file Is then plotted using a solid line for clean sands and a dotted line for silty sands and silts as shown in Figure 32.

Seismicity

The ground motion characteristics of a site affect both liquefaction opportunity and susceptibility. Liquefaction opportunity is the probability of a certain ground acceleration being exceeded in the time period of interest. Although earthquake magnitude affects the intensity of ground accelerations, magnitude itself is not directly expressed in the opportunity. However, the values of expected earthquake magnitude are included in the analysis by using the values in calculating opportunity as well as critical acceleration values of the liquefaction susceptibility.

Cone Sounding 27
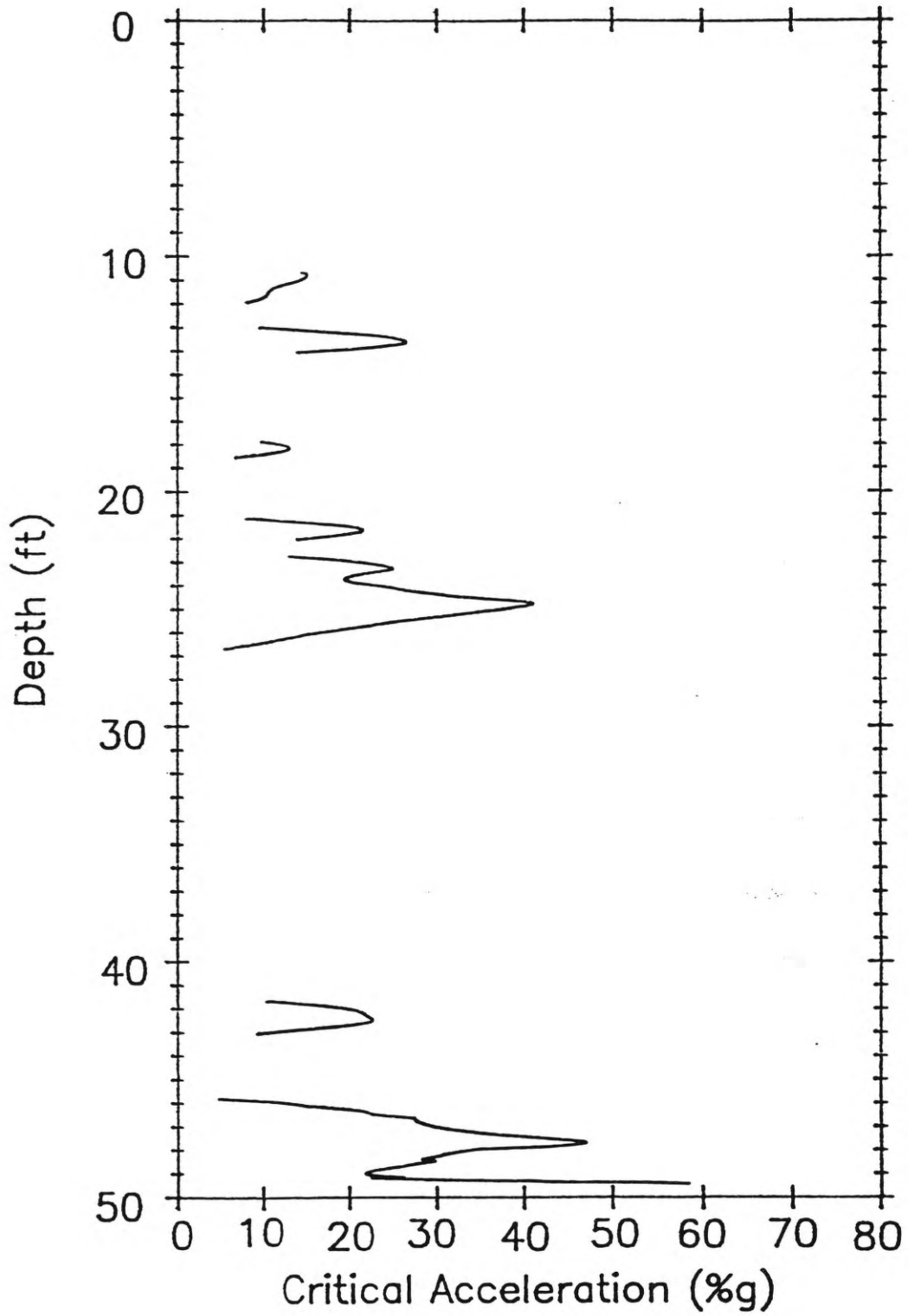
Figure 32. Example of output from PCRACCO.

Exceedence probability curves

The probability of an acceleration value being exceeded is determined by first calculating the number of occurrences per year of accelerations equal to or greater than the value of interest (annual occurrence rate) and then using the following relationship to calculate the exceedence probability (Haley and Hunt, 1974):

$$P = 1-e^{-tN/T} \tag{13}$$

P = probability of at least one occurrence in time period t
t = time period of interest
N = number of occurrences in time period T
T = time period used in recurrence rate (1 year).

In this study, the annual occurrence rate was calculated for a range of ten different acceleration values using the programs EQRISK (McGuire, 1976) and FRISK (McGuire, 1978). EQRISK calculates the acceleration occurrences from earthquakes in source areas while FRISK calculates the acceleration occurrences from earthquakes along specific faults. The exceedence probability in a 100 year period for each of the ten acceleration values was then calculated using Equation 13. A curve was then fit through the ten points so that acceleration values corresponding to 50, 10 and 5 percent exceedence probability in 100 years could be picked off the plot. These acceleration values correspond to boundaries between high, moderate, low and very low liquefaction potential.

The analysis described above was performed for 23 locations throughout the study area. Nine source areas were considered to calculate the background seismicity

using EQRISK while FRISK was used to model the seismicity from the ten segments of the Wasatch fault. The seismicity parameters for the source areas and fault segments used in the analysis are presented in Appendix B.

Figure 33 is a plot of acceleration versus annual occurrence rate for a site near Salina. Figure 34 is an exceedence probability curve for the same site. The critical accelerations corresponding to 50, 10 and 5 percent exceedence probability are indicated on Figure 34. The accelerations corresponding to the previously mentioned exceedence values for all 23 sites are presented in Table 5. Appendix C contains the annual occurrence rate and exceedence probability curves for the 22 other sites analyzed.

Study of Table 5 reveals there are very small changes in acceleration probabilities between adjacent sites. Therefore, it is possible to group several sites into areas and use representative values of acceleration for the entire group. The acceleration values for the areas used are presented in Table 6.

Location 8–Salina
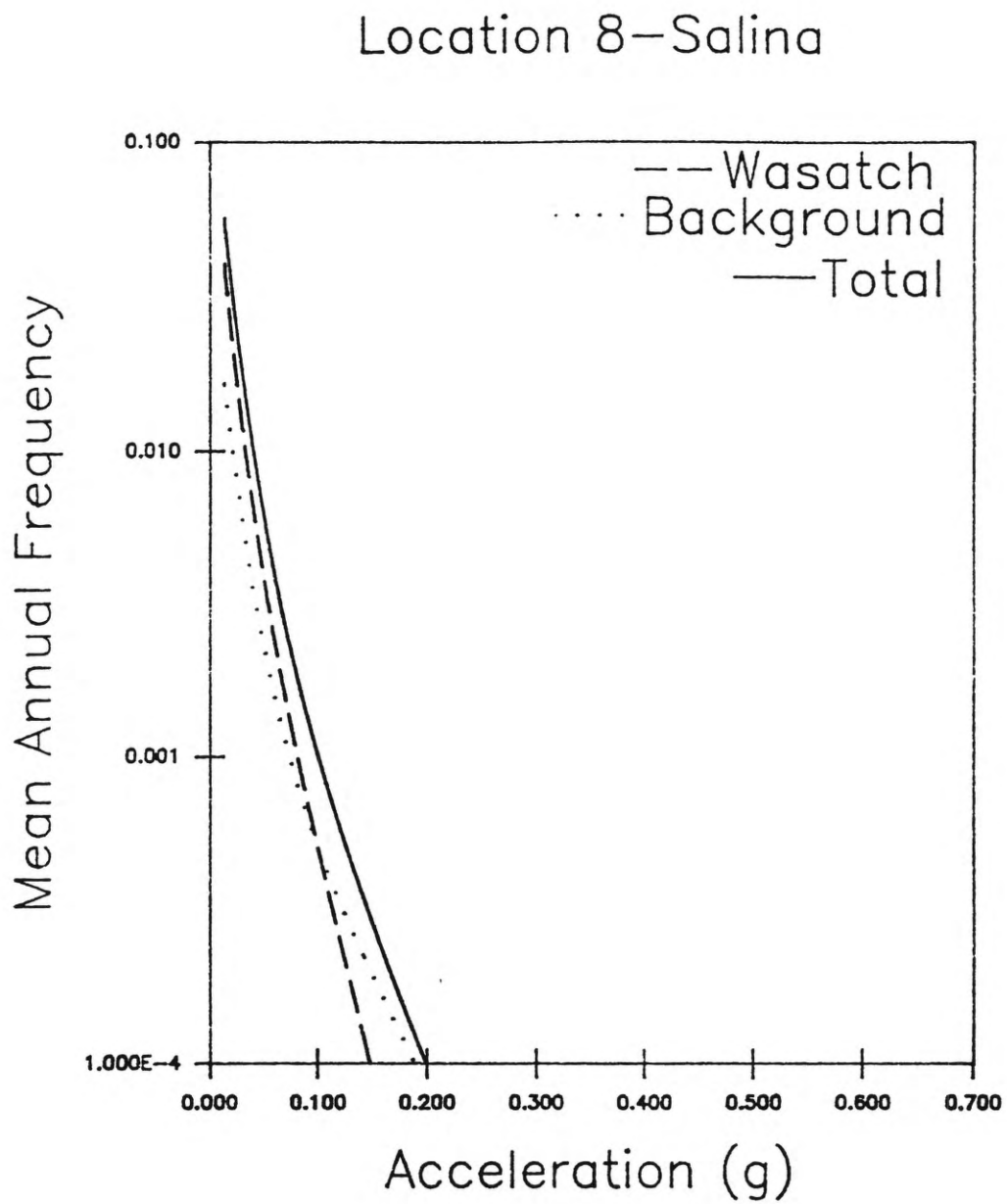
Figure 33. Annual occurrence rate versus acceleration for Salina.

80
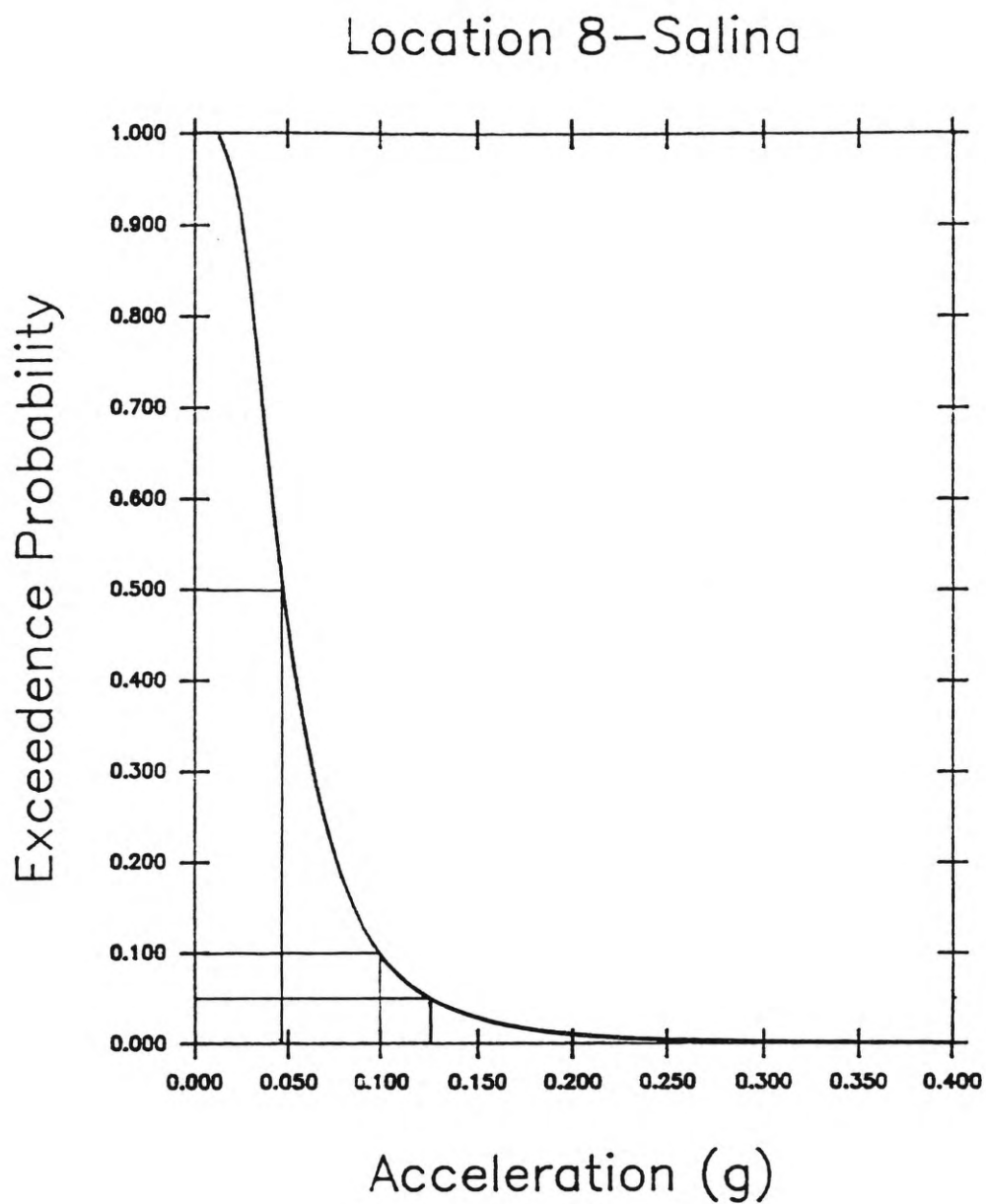
Location 8–Salina

Figure 34. 100 year exceedence probability curve for Salina.

Table 5. Accelerations corresponding to 50, 10 and 5 percent
exceedence probability for sites throughout the study area.

Location Number	Location	Acceleration corresponding to probability 50%	10%	5%
1	Park City	.14	.225	.26
2	Heber	.13	.19	.22
3	Sevier	.03	.07	.09
4	Monroe	.04	.115	.16
5	Elsinore	.04	.11	.16
6	Richfield	.04	.105	.145
7	Aurora	.045	.09	.13
8	Salina	.05	.10	.13
9	Centerfield	.06	.135	.17
10	Fayette	.07	.17	.22
11	Manti	.07	.14	.175
12	Ephram	.085	.18	.215
13	Chester	.09	.17	.19
14	Nephi	.205	.32	.37
15	West of Nephi	.175	.275	.32
16	Mona	.22	.34	.40
17	Levan	.155	.265	.315
18	Chicken Cr. Res.	.13	.26	.31
19	Mills Valley	.085	.20	.24
20	Delta	.04	.07	.08
21	Fillmore	.05	.105	.13
22	Kanosh	.04	.08	.11
23	Scipio	.065	.145	.18

Table 6. Representative accelerations corresponding to 50, 10 and 5 percent exceedance probabilities in 100 years for regions of the study area.

Region	Accelerations Corresponding to Probability		
	50%	10%	5%
Park City-Heber	.07	.17	.22
Juab Valley	.08	.26	.40
Mills Valley	.04	.12	.16
Sanpete Valley	.04	.14	.18
N. Sevier Valley	.03	.11	.15
S. Sevier Valley	.08	.24	.30
Pavant Valley/ Sevier Desert	.04	.10	.13
Scipio Valley	.04	.12	.16

Determining design magnitude

As previously discussed, the critical acceleration required to cause liquefaction is affected considerably by the magnitude of the earthquake producing the ground motions. Therefore, it is important to determine the magnitude of the earthquake likely to produce the critical acceleration.

Referring to Figure 33, one can see that at the higher acceleration values the background earthquake accounts for most of the risk of these values being exceeded.

Since the higher acceleration values are responsible for the liquefaction risk, the background earthquake is used as the design earthquake in this case. The maximum magnitude of a background earthquake is considered to be 6.5. Thus, this value will be used as the design earthquake for the Salina area. The design magnitudes used in this study are presented in Table 7.

Determining Liquefaction Potential Zones

Once critical accelerations were determined for each of the data points, they were plotted on base maps. In earlier studies along the Wasatch Front there was sufficient data to delineate the boundaries between liquefaction potential zones by contouring the acceleration values along the values corresponding to the different potential classifications (i.e., high, moderate, low and very low). The boundaries were then adjusted to match the local geomorphic features. However, due to the sparse data in this study, the geomorphic features were relied on much more to determine the boundary locations.

In most areas a boundary was drawn along the 10 feet depth to ground water contour. This boundary usually defined a region in the center of the valley with shallow ground water conditions. The critical accelerations in this region were then used to determine the liquefaction potential in the shallow ground water area. Other boundaries were then added by contouring critical accelerations within the shallow ground water

Table 7. Design magnitudes used in calculating critical accelerations.

Region	Design Magnitude
Juab Valley	7.25
Sevier Bridge Reservoir to Gunnison	7.0
Sevier Valley; Gunnison to Richfield	6.5
Sevier Valley; south of Richfield	7.0
Sanpete Valley	6.5
Mills and Little Valleys	7.0
Scipio and Round Valleys	6.5
Pavant Valley/ Sevier Desert	6.25

region or by adding zones with lower liquefaction probability outside the shallow ground water region where change in depth to water was gradual. Other boundaries were added where appropriate around geomorphic features where critical accelerations indicated a change in liquefaction probability.

After boundaries were drawn on the map using the procedure described above, a trip to the study area was to confirm or adjust the boundaries. In the field the soil, ground water and geologic conditions could be observed in more detail and the boundaries adjusted to better fit the field conditions.

RESULTS AND CONCLUSIONS

Liquefaction Potential Maps

Plates 1 through 14 are the liquefaction potential maps for the study area. The areas on the maps have been divided into moderate, low and very low liquefaction potential zones since none of the areas were found to contain deposits with high liquefaction probability. Due to the extreme scarcity of data in some areas, dashed lines were used to indicate the boundaries between zones. These dashed lines indicate an inferred boundary that could not be determined accurately enough to justify a solid line boundary.

The following text contains discussion pertaining to the liquefaction potential in each of the regions of the study. This text should be used as a guide when using the maps of Plates 1 through 14 to give the user further insight into the subsurface conditions and the interpretation of the results.

Park City-Heber area

The Park City-Heber area (Plate 1) contains a few small areas with low liquefaction potential and one strip along the Provo River with moderate liquefaction potential. The remainder of the area is considered to have very low liquefaction potential.

In the Park City area, the lower sections of Park City and an area extending

northward into a small alluvial valley are classified as a region with low liquefaction potential. A small area to the east is also classified as such. This classification is based on a number of borings indicating critical accelerations in the low probability range. Although there are a few borings that indicated moderate liquefaction potential and others indicating very low potential, most critical acceleration values are close to the low potential range and the low classification is considered indicative of the conditions in the entire zone.

The Parleys Park area, north of Park City, was found to have very low liquefaction potential due to most deposits consisting of dense gravel.

The Heber Valley is divided into three zones. A zone along the Provo River running through the middle of the valley is classified having moderate liquefaction potential. This classification is based on a set of borings east of Midway and experience from past studies that indicate flood-plain deposits are generally liquefiable. The east half of the valley is classified as very low due to the existence of large cobbles and gravel in the subsurface. The area around Midway is also classified as very low due to the tufa deposits from the hot springs cementing the sediments.

Due to the absence of data, the Provo River canyon area was left unclassified. However, it would be expected to have low or very low liquefaction potential due to the existence of boulders and cobbles that are found washed into the northern part of Heber Valley.

Juab Valley

Northern Juab Valley. In northern Juab Valley (Plate 2) the ground water data of Bjorklund (1967) was used to draw a contour around the area having ground water at a depth less than ten feet below the ground surface. Inside this region two cone penetrometer soundings and one boring had layers with critical acceleration that indicated exceedence probabilities ranging from moderate to barely over the moderate-high probability boundary. The layers indicating high liquefaction probability are very thin (one foot or less) while sand layers of considerable thickness had critical accelerations in the moderate exceedence probability zone.

Since the likelihood of liquefaction in thin layers being manifested at the relatively level valley floor is very small, the risk due to the thin layers is considered to be greatly reduced. Therefore, the greatest risk, with regard to liquefaction, is due to the layers having critical accelerations in the moderate exceedence probability range. Thus, the zone is given a moderate liquefaction potential classification as indicated on Plate 2.

Southern Juab Valley. In southern Juab Valley (Plate 3) the ground water data of Bjorklund and Robinson (1968) was used to identify the shallow ground water region. Critical accelerations within this region indicate a general decrease in liquefaction potential towards the lower portion of the valley around Chicken Creek Reservoir. A distinct geomorphic feature, the flat area around Chicken Creek Reservoir containing numerous springs, is classified as having moderate liquefaction potential. This

classification is supported by the critical acceleration data of the set of borings in the southeast portion of the zone. Areas outside the moderate zone but still in the shallow ground water zone are classified as having low liquefaction potential.

Mills and Little Valleys

The bottom of Mills Valley consists of flood-plains, oxbow lakes and abandoned stream channels of the Sevier River. Two sets of borings in the valley indicate moderate liquefaction potential exists throughout the valley as indicated on Plate 4. The bottom of the canyon leading to Chicken Creek Reservoir is also classified as moderate.

Due to deep ground water conditions, Little Valley is classified as having very low liquefaction potential.

Sanpete Valley

The valley fill of the central area of Sanpete Valley is a heterogeneous mix of sands, silts and clays. Robinson (1971) reported that geophysical logs indicate thick beds could be traced across the valley; however, the material in these beds is arranged in lenticular, discontinuous deposits of varying soil types. The data from the supplemental field study supports this interpretation. Soil types encountered in the study include sands, silts, clays and peat and critical accelerations indicate liquefaction potential ranging from moderate to very low.

The shallow ground water boundary (depth to water less than ten feet) defined by Robinson (1971) is used to delineate the zone of liquefiable material (Plates 5 and 6). Due to the heterogeneous nature of the valley fill, it is not possible to break the valley down into smaller zones. Instead, the entire shallow ground water zone is classified as locally variable with low to moderate liquefaction potential. When development of any portion of this area is being considered, the site specific analysis requirement matrix of Table 4 should be used along with good engineering judgement to determine the type of site specific investigation required.

In the small valleys south of Manti specific classifications were assigned based on one set of borings in each valley. Arapian Valley, ten miles south of Manti, is classified as having very low liquefaction potential based on the ground water data of Robinson (1971). These areas are shown on Plate 7.

Sevier Valley

Northern Sevier Valley. Northern Sevier Valley (Plate 7) is defined in this study as the area north of the Sanpete-Sevier County line. Deposition of the sediments in the central region has been dominated by the processes of the Sevier River. As indicated by the ground water levels encountered in the borings of the area, the location of the flood-plain of the Sevier River corresponds fairly well with the location of the shallow ground water zone. The only major exception to this is where the ground water level is

raised due to the effect of the San Pitch River entering the valley. Thus due to the usually high liquefaction susceptibility of river sediments combined with shallow ground water conditions, the shallow ground water area is used to define the zone of liquefiable deposits.

Critical accelerations calculated in the liquefiable zone indicate low liquefaction potential in the region south of Gunnison and moderate liquefaction potential north of Gunnison. An increase in liquefaction opportunity as the distance to the Wasatch fault zone decreases also supports the reasoning for this trend. Therefore, since no sharp boundary separates the southern and northern regions, the southern region is classified as having low liquefaction potential which grades to moderate east of Gunnison. The area north of Gunnison is classified as a moderate liquefaction potential zone.

Southern Sevier Valley. The deposits of southern Sevier Valley (south of Sanpete-Sevier County line) are also dominated in the lower regions by the depositional processes of the Sevier River. The shallow ground water zone was determined by extrapolation of the water table data in the borings of the area. The shallow ground water zone was found to approximately coincide with the flood-plain of the Sevier River as was the case in the northern section of the valley. Therefore, due to the susceptibility of river deposits to liquefaction and the shallow ground water condition, the shallow ground water zone was determined to be a zone of liquefiable deposits.

Critical accelerations within the shallow ground water zone indicate moderate

liquefaction potential in the southern part of the valley from Central to Rocky Ford Dam, north of Sigurd. In the vicinity of Rocky Ford Dam the liquefaction potential grades to low and is classified as low northward to the county line. These classifications are shown on Plates 8 and 9.

South of Rocky Ford Dam, on the west side of the valley, the slope of the valley is gradual enough so that the depth to ground water drops off slowly. The result is a zone with moderate depth to ground water. Critical accelerations in this region indicate low liquefaction potential. In the southern end of the valley this zone is extended to a wider zone of moderate depth to ground water and also along the Sevier River to the extreme southern end of the valley.

It is worth noting that in 1901, during an earthquake (magnitude estimated at 7.0) in the Richfield area, sands liquefied and were ejected at the ground surface near the Sevier River channel. This occurred in an area three miles east of Richfield that is included in the moderate liquefaction potential zone (Williams and Tapper, 1953).

Pavant Valley

Most of the Pavant Valley area (Plates 10 and 11) is a region with deep ground water and, thus, very low liquefaction potential. The shallow ground water belt identified by Meinzer (1911) is the only area in the valley with ground water at a depth of less than 30 feet. However, borings in the shallow ground water belt indicate the deposits are

dense and, therefore, not susceptible to liquefaction. The lack of susceptible deposits combined with low liquefaction opportunity in the area renders the entire Pavant valley with a very low liquefaction potential classification.

Sevier Desert

The sediments on the valley floor of the Sevier Desert are the result of the depositional processes of the Sevier River and Lake Bonneville. The result of this depositional environment is an area with heterogeneous deposits consisting of discontinuous beds of sand, silt and clay.

Boring logs in the valley floor area indicate low to very low liquefaction potential and ground water at depths less than ten feet. The ground water data of Mower and Feltis (1968) is used to define the boundary of the shallow ground water region and, thus, the boundary of the low liquefaction potential zone (Plate 12). The dune sands along the eastern edges of the valley are classified as a very low liquefaction zone due to deep ground water conditions.

The Sevier River flood-plain from Delta through Leamington Canyon to Mills Valley is classified as a low liquefaction potential zone (Plates 4, 12 and 13). This classification is supported by critical accelerations from several borings near Delta and past experience indicating liquefaction susceptibility of flood-plain deposits. As Leamington Canyon leads out from Mills Valley the moderate liquefaction potential in Mills Valley

grades to a low classification in the canyon. This gradational boundary is based on the critical accelerations near Delta and also the decrease in liquefaction opportunity to the west moving away from the Wasatch fault zone.

Scipio Valley

Bjorklund and Robinson (1968) identified a shallow ground water region in the center of Scipio Valley. This shallow ground water region ends abruptly north of Scipio due to sink holes draining the ground water to a depth of over 100 feet. Borings in the area indicate silts and silty sands with critical accelerations in the low exceedence probability range exist in this region. Thus, the shallow ground water region is classified as a low liquefaction potential zone as indicated on Plate 14.

Due to a lack of subsurface information, Round Valley, north of Scipio, was left unclassified. The shallow ground water region around Scipio Lake could contain deposits with low liquefaction potential, thus, it is recommended that a site specific investigation be conducted before any critical structures are constructed in the area.

Conclusions

Although deposits susceptible to liquefaction were found to exist in the study area, the potential for liquefaction in the study area is much lower than along the Wasatch

Front due to decreased seismic activity lowering the liquefaction opportunity of the area. Nonetheless, there are numerous regions in the study area with moderate liquefaction potential and still many others with low liquefaction potential. Albeit, the risk due to liquefaction is less than was found in other study areas, the risk is still significant and should be considered in planning, especially when dealing with critical structures.

The lack of data available in the study area affected the precision with which the boundaries could be determined. However, the geomorphic features proved to be a very valuable tool for defining boundary locations and there is no reason to believe that the maps produced in this study are any less reliable than the ones produced in the previous studies along the Wasatch Front. In several areas the classifications are more ambiguous than those found in the previous studies, however, this is more a consequence of heterogeneous valley fill rather than a lack of data.

LITERATURE CITED

ASCE (American Society of Civil Engineers). 1978. Definition of terms related to liquefaction. Journal of the Geotechnical Engineering Division, ASCE. 104(GT9):1197-1200.

Anderson, L.R. and J.R. Keaton. 1982. Development of a soil liquefaction potential map. A paper presented at the International Conference on Soil Dynamics and Earthquake Engineering. Southhampton, England.

Anderson, L.R., J.R. Keaton, K. Aubrey and S.J. Ellis. 1982. Liquefaction potential map for Davis County, Utah. Report to the U.S. Geological Survey by Utah State University, Logan, Utah.

Anderson, L.R., J.R. Keaton and J.A. Bay. 1987. Liquefaction potential map for Weber, Box Elder, and Cache counties, Utah. Report to the U.S. Geological Survey by Utah State University, Logan, Utah.

Anderson, L.R., J.R. Keaton, J.A. Bay and J.D. Rice. 1987. Soil liquefaction potential mapping along the Wasatch Front. pp 1-17, Proceedings of the 23rd Symposium on Engineering Geology and Soils Engineering, Logan, Utah.

Anderson, L.R., J.R. Keaton and J.E. Bischoff. 1986a. Liquefaction potential map for Utah County, Utah. Report to the U.S. Geological Survey by Utah State University, Logan, Utah.

Anderson, L.R., J.R. Keaton, J. Spitzley and A. Allen. 1986b. Liquefaction potential map for Salt Lake County, Utah. Report to the U.S. Geological Survey by Utah State University, Logan, Utah.

Anderson, L.W. and D.G. Miller. 1979. Quaternary faulting in Utah: In Proceedings of Conference X, Earthquake Hazards Along the Wasatch and Sierra-Nevada Frontal Fault Zones, National Earthquake Hazards Reduction Program, 1979. U.S. Geological Survey Open File Report 80-801, pp 194-226.

Anderson, R. E. 1988. Personal Communication, U. S. Geological Survey, Denver Colorado.

Arabasz, W. J. 1988. Personal Communication, Department of Geology and Geophysics, University of Utah, Salt Lake City, Utah.

Arabasz, W.J., R.B. Smith and W.D. Richins. 1979. Earthquake studies in Utah, 1850 to 1978. University of Utah Seismograph Stations, Department of Geology and Geophysics, University of Utah, Salt Lake City, Utah.

Bay, J. A. 1987. Liquefaction potential mapping of Weber, Box Elder and Cache Counties, Utah. Unpublished M.S. Thesis. Utah State University, Logan, Utah.

Bjorklund, L. J. 1967. Ground water resources of northern Juab Valley, Utah: Utah Department of Natural Resources Technical Publication 17.

Bjorklund, L. J. and G. B. Robinson. 1968. Ground-water Resources of the Sevier River Basin between Yuba Dam and Leamington Canyon, Utah: U. S. Geological Survey Water-Supply Paper 1848.

Castro, G. and S. J. Poulos. 1977. Factors affecting liquefaction and cyclic mobility. Journal of the Geotechnical Engineering Division, ASCE. 103(GT6):501-506.

Chameau, J. L. and G. W. Clough. 1983. Probabilistic pore pressure analysis for seismic loading. Journal of the Geotechnical Engineering Division, American Society of Civil Engineers. 109(4):507-524.

Crittenden, M. D. 1963. New data on the isostatic deformation of Lake Bonneville: U. S. Geological Survey Prof. Paper 454-E.

DeAlba, P., H. B. Seed and C. K. Chan. 1976. Sand liquefaction in large-scale simple shear tests. Journal of the Geotechnical Engineering Division, ASCE. 102(GT9):909-927.

Dobrey, R., K. H. Stokoe II, R. S. Ladd and T. L. Youd. 1981. Liquefaction Susceptibility from S-wave Velocity. ASCE National Convention, St. Louis, Missouri, October 1981. ASCE, New York, New York. Preprint 81-544.

Douglas, B. J. and R. S. Olsen. 1981. Soil classification using the electric cone penetrometer, p. 209-227. In Proceedings of Symposium on Cone Penetration Testing and Experience, Geotechnical Engineering Division, ASCE, St. Louis.

Eardley, A. J., Gvosdetsky, Vasyl and Marsel. 1957. Hydrology of Lake Bonneville and sediments and soils of its basin. Geological Soc. America Bill., v. 68, p. 1141-1202.

Grantz, A., G. Plafker and R. Kachadoorian. 1964. Alaska's Good Friday Earthquake, March 27, 1964. Geological Survey Circular 491, Department of the Interior, Washington, D.C..

Haley, S. C. and G. S. Hunt. 1974. Determination of design earthquake characteristics. American Society of Civil Engineers National Meeting on Water Resources Engineering: Meeting Preprint 2183.

Hintze, L. F. 1973. Geological History of Utah. Department of Geology, Brigham Young University, Provo, Utah.

Kavazanjian E., R. A. Roth and H. Echezuria. 1985. Liquefaction potential mapping for San Francisco. Journal of Geotechnical Engineering, ASCE. 111(1):54-76.

Machette M. N., S. F. Personius, A. R. Nelson. 1987. Quaternary geology along the Wasatch Fault Zone: segmentation, recent investigations, and preliminary conclusions. p. A1-72. In Assessment of Regional Earthquake Hazards and Risk Along the Wasatch Front, Utah: U. S. Geological Survey Open-File Report 87-585.

McGuire R. K. 1976. FORTRAN computer program for seismic risk analysis. U. S. Geological Survey Open-File Report 76-67.

McGuire R. K. 1978. FRISK: computer program for seismic risk analysis using faults as earthquake sources. U. S. Geological Survey Open-File Report 78-1007.

Meigh, A. C. 1987. Cone penetration testing. Butterworths, Boston, Massachusetts.

Meinzer, O. E. 1911. Ground water in Juab, Millard and Iron Counties, Utah. U. S. Geological Survey Water Supply Paper 277.

Mower R. W. and R. D. Feltis. 1968. Ground-water hydrology of the Sevier Desert, Utah. U. S. Geological Survey Water-Supply Paper 1854.

NRC (National Research Council), Committee on Earthquake Engineering. 1985. Liquefaction of soils during earthquakes. National Academy Press, Washington, D.C.

Robertson, P. K. 1985. In-situ testing and its application to foundation engineering. 1985 Canadian Geotech. Colloquium, Canadian Geotech. Journal, v. 23, no. 23.

Robertson P. K. and R. G. Campanella. 1986. Guidelines for use, interpretation and application of the CPT and CPTU. Hogentogler and Company, INC.

Robinson G. B. 1971. Ground water hydrology of the San Pitch River drainage basin, Sanpete County, Utah. U. S. Geological Survey Water-Supply Paper 1896.

Schmertmann, J. H. 1977. Guidelines for cone penetration test performance and design. FHWA-TS-78-209. Federal Highway Administration, Offices of Research and Development, Implementation Division, Washington, D.C.

Seed, H. B. 1979. Soil liquefaction and cyclic mobility evaluation for level ground during earthquakes. Journal of the Geotechnical Engineering Division, ASCE. 105(GT2):201-255.

Seed, H. B. and I. M. Idriss. 1967. Analysis of soil liquefaction: Niigata Earthquake. Journal of the Soil Mechanics and Foundation Division, ASCE. 93(SM3):83-108.

Seed, H. B. and Idriss. 1971. Simplified procedure for evaluating soil liquefaction potential. Journal of the Soil Mechanics and Foundation Division, ASCE. 97(SM9):1249-1273.

Seed, H. B. and I. M. Idriss. 1982. Ground motions and soil liquefaction during earthquakes. Monograph Series, Earthquake Engineering Research Institute, Berkeley, California.

Seed, H. B., I. M. Idriss and I. Arango. 1983. Evaluation of liquefaction potential using field performance data. Journal of the Geotechnical Engineering Division, ASCE. 109(GT3).

Seed, H.B. and K.L. Lee. 1966. Liquefaction of saturated sands during cyclic loading. Journal of the Soil Mechanics and Foundation Engineering Division, ASCE. 92(SM6):105-134.

Seed, H. B., K. Mori and C. K. Chan. 1977. Influence on the seismic history on liquefaction of sand. Journal of the Geotechnical Engineering Division, ASCE. 109(GT3).

Seed, H. B. and W. H. Peacock. 1971. Test procedure for measuring soil liquefaction characteristics. Journal of the Geotechnical Engineering Division, ASCE. 97(SM8):1099-1119.

Seed, H. B., K. Tokimatsu, L. F. Harder and R. M. Chung. 1985. Influence of SPT procedures in soil liquefaction resistance evaluation. Journal of the Geotechnical Engineering Division, ASCE. 111(GT12):1425-1444.

Stripeika, C. 1988. (Untitled at time of this writing). Unpublished M.S. Thesis, Utah State University, Logan, Utah. (in progress).

Tinsley, J. C., T. L. Youd, D. M. Perkins and A. T. F. Chen. 1985. Evaluating liquefaction potential. p. 263-315 In Evaluating Earthquake Hazards in the Los Angeles Region - An Earth Science Perspective: U. S. Geological Survey Professional Paper 1360.

Williams, J. S. and M. L. Tapper, 1953. Earthquake history of Utah, 1850-1949. Seismological Society of America Bulletin, v. 43, p.191-218.

Youd, T. L. 1972. Compaction of sands during repeated straining. Journal of the Soil Mechanics and Foundation Engineering Division, ASCE. 90(SM7):709-725.

Youd, T. L. 1973. Liquefaction, flow and associated ground failure. U. S. Geological Survey Circular 688.

Youd, T. L. 1978. Major cause of earthquake damage is ground failure. Civil Engineering, ASCE. 48(4):47-51.

Youd, T. L. and D. M. Perkins. 1978. Mapping liquefaction induced ground failure potential. Journal of the Geotechnical Engineering Division, ASCE. 104(GT4):433-446.

Youd, T. L. and D. M. Perkins. 1987. Mapping of liquefaction severity index. Journal of the Geotechnical Engineering Division, ASCE. 113(GT11):1364-1392.

Young, R. A. and C. H. Carpenter. 1965. Ground-water conditions and storage in the central Sevier Valley, Utah. U. S. Geological Survey Water-Supply Paper 1787.

Young, R. R., F. H. Swan, M. S. Power, D. P. Schwartz and R. K. Green. 1987. Probabilistic analysis of earthquake ground shaking hazard along the Wasatch Front, Utah. p. M1-110 In Assessment of Regional Earthquake Hazards and Risk Along the Wasatch Front, Utah: U. S. Geological Survey Open-File Report 87-585.

APPENDICES

Appendix A. Soil Data

Table 8. Soil data for clean sands $D_{50} > 0.25$ mm.

Sample	N	Q_c (tons/ft sq)	F_r %	Unified Soil Class	Q_c/N
BH 3-1	8	52	1.4	SP	6.5
BH 6-8	79	215	1.0	SP-SM	2.7
BH 16-6	13	76	0.9	SP-SM	5.8
BH 16-7	14	140	1.0	SP	10.0
BH 19-1	26	150	1.0	SP	5.8

Table 9. Soil data for silty sands $0.15 < D^50 < 0.25$ mm.

Sample	N	Q_c (tons/ft sq)	F_r %	Unified Soil Class	Q_c/N
BH 2-4	7	117	1.1	SM	16.7
BH 2-5	17	48	4.8	ML	2.8
BH 3-2	3	150	1.1	ML	50.0
BH 3-3	6	15	1.9	ML	2.5
BH 3-12	11	39	2.1	SM	3.5
BH 6-3	13	21	2.4	ML	1.6
BH 6-7	10	32	6.2	SM	3.2
BH 8-1	6	6	2.5	ML	1.0
BH 8-2	5	26	3.0	ML	5.2
BH 8-3	7	20	3.0	ML	2.9
BH 10-10	8	60	2.0	ML	7.5
BH 16-12	22	92	1.6	SM	4.2
BH 19-4	45	190	3.1	SM	4.2
BH 23-6	5	30	3.0	ML	6.0
BH 23-8	8	11	5.7	SM	2.5

Table 10. Soil data for clays and plastic silts (non-liquefiable soils).

Sample	N	Q_c (tons/ft sq)	F_r %	Unified Soil Class	Q_c/N
BH 2-1	8	25	4.0	CL-CH	3.1
BH 2-3	17	21	7.3	MH	1.2
BH 3-4	5	8	3.4	CL	1.6
BH 3-5	4	15	2.6	CL-ML	3.7
BH 3-7	8	21	3.0	CL	2.6
BH 3-9	8	35	3.0	CL-ML	4.4
BH 3-10	5	15	3.5	CL-CH	3.0
BH 6-1	5	6	4.0	CL	1.2
BH 6-4	7	14	4.1	ML	2.0
BH 8-4	3	3	4.8	CL-ML	1.0
BH 10-1	4	5	4.3	CL	1.2
BH 10-2	10	12	5.4	CL-CH	1.2
BH 10-3	14	20	7.6	CL-CH	1.4
BH 10-4	9	10	8.1	CL	1.1
BH 10-6	8	10	8.0	CL	1.2
BH 10-8	10	19	7.0	CL-CH	1.9
BH 10-9	8	40	3.3	CL-ML	5.0
BH 10-12	8	12	4.7	CL	1.5
BH 10-13	6	9	4.4	CL	1.5
BH 14-1	8	11.	5.0	CL	1.4
BH 14-2	6	8	2.7	CL	1.3
BH 14-4	5	16	3.0	CL-ML	3.2
BH 14-5	3	13	1.2	CL	4.3
BH 14-6	9	26	3.8	CL-ML	3.2
BH 14-7	15	30	4.2	CL-CH	2.0
BH 14-8	12	12	3.3	CL-ML	1.0
BH 14-9	12	17	7.0	CL-ML	1.4
BH 16-1	4	8	3.6	CL-ML	2.0

Table 10. (Continued)

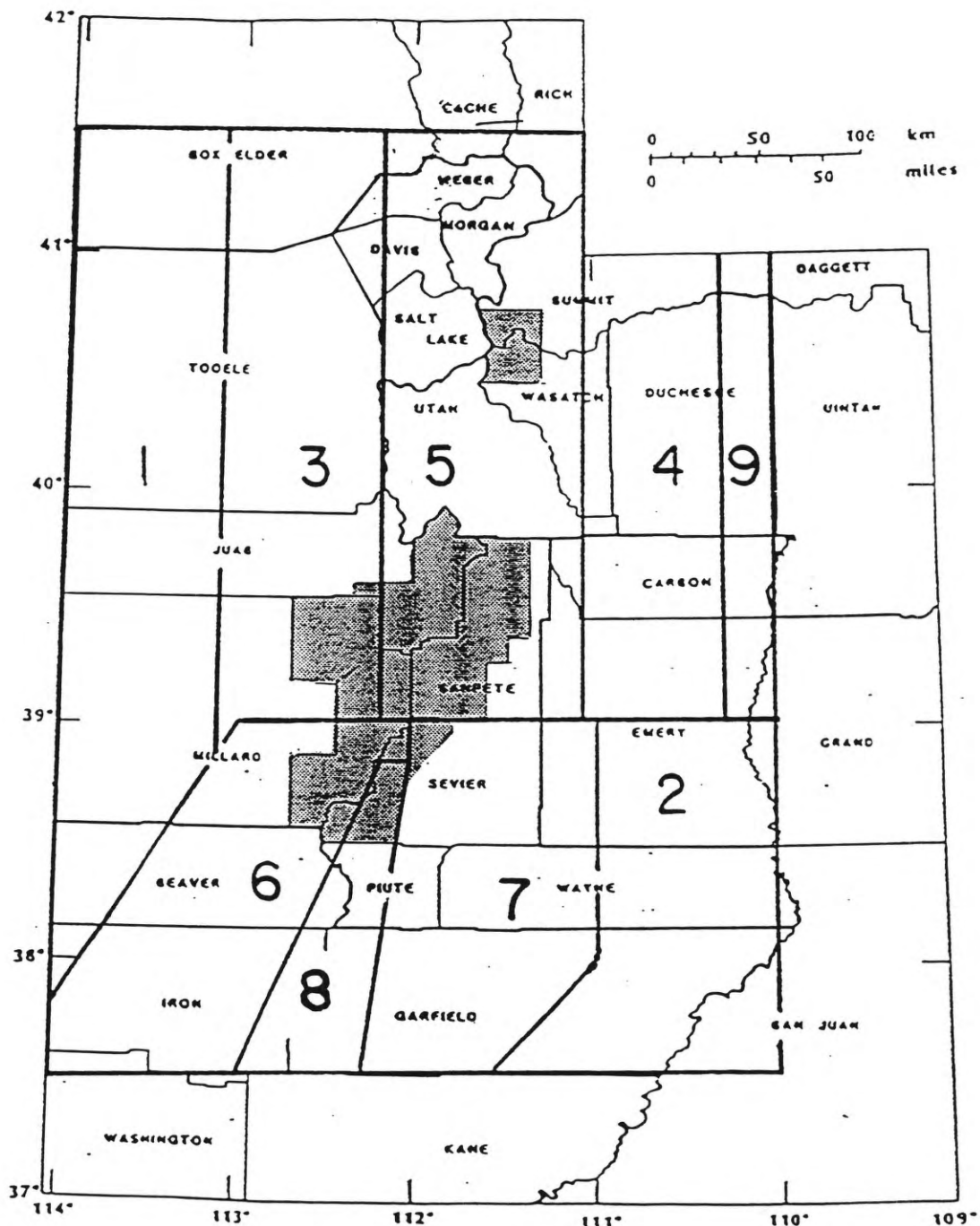| Sample	N	Q_c (tons/ft sq)	F_r %	Unified Soil Class	Q_c/N
BH 16-3	1	5	1.5	MH	5.0
BH 16-4	1	5	2.5	CL	5.0
BH 16-8	5	15	2.4	CL	3.0
BH 16-10	3	7	3.4	OH	2.3
BH 23-2	5	7	3.9	CL-ML	1.4
BH 23-3	4	7	5.2	MH	1.7
BH 23-9	12	17	6.8	CH	1.4
BH 23-10	12	14	5.9	CL-ML	1.2

Appendix B. Seismic Parameters

Figure 35. Source areas used in determining background seismicity values for study area.

Table 11. Input parameters for EQRISK for source areas of Figure 35.

Source Area	M_O	M1	b	Rate/yr.	Focal Depth	Area (km^2)
1	4.0	6.25	0.71	0.0440	7.5	28075
2	4.0	6.25	0.71	0.0440	7.5	16195
3	4.0	6.25	0.71	0.0570	7.5	9676
4	4.0	6.25	0.71	0.0570	7.5	24393
5	4.0	6.25	0.71	0.0290	7.5	22790
6	4.0	6.50	0.71	0.0290	7.5	17190
7	4.0	6.50	0.71	0.0320	7.5	14080
8	4.0	7.0	0.71	0.0292	10.0	5318
9	4.0	6.5	0.71	0.0440	7.5	5497

Table 12. Input parameters for FRISK for segments of the Wasatch fault.

Segment Number	Segment Name	M_{min}	M_{max}	Rate	b	Depth (km)
1	Collinston	6.0	7.36	0.0006	0.50	0.000
2	Brigham City	6.0	7.14	0.0006	0.50	0.000
3	Weber	6.0	7.29	0.0053	0.50	0.000
4	Salt Lake	6.0	7.25	0.0026	0.50	0.000
5	American Fork	6.0	7.84	0.0024	0.50	0.000
6	Provo	6.0	7.84	0.0025	0.50	0.000
7	Spanish Fork	6.0	7.09	0.0028	0.50	0.000
8	Nephi	6.0	7.14	0.0045	0.50	0.000
9	Levan	6.0	7.11	0.0011	0.50	0.000
10	Fayette	6.0	6.64	0.0003	0.50	0.000

Appendix C. Mean Annual Frequency and Exceedence Probability Curves.
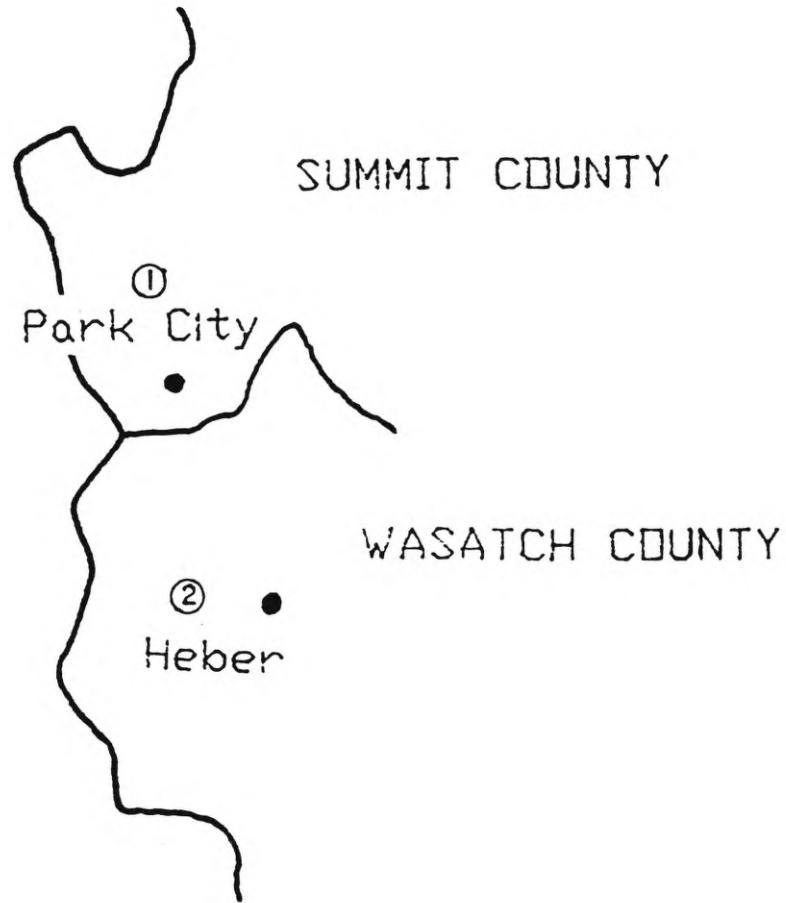
Figure 36. Locations of seismic analysis in northern section of study area.
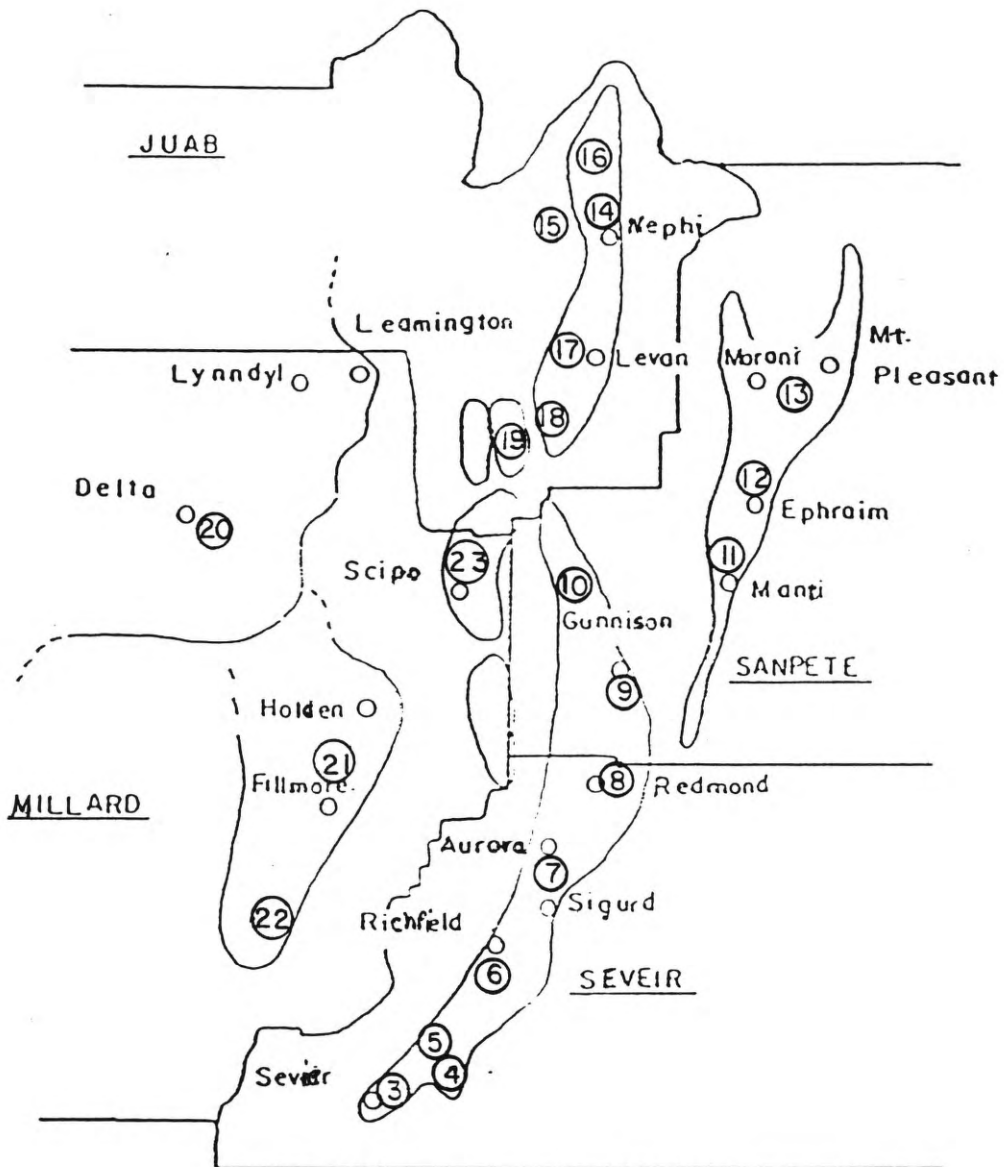
Figure 37. Locations of seismic analysis in southern section of study area.

Location 1—Park City

Location 1—Park City

Location 2—Heber

Location 2—Heber

Location 3—Sevier

Location 3—Sevier

Location 4—Monroe

Location 4—Monroe

Location 5—Elsinore

Location 5—Elsinore

Location 6—Richfield

Location 6—Richfield

Location 7—Aurora

Location 7—Aurora

Location 8—Salina

Location 8—Salina

Location 9—Centerfield

Location 9—Centerfield

Location 10—Fayette

Location 10—Fayette

Location 11—Manti

Location 11—Manti

Location 12-Ephram

Location 12-Ephram

Location 13—Chester

Location 13—Chester

Location 14–Nephi

Location 14–Nephi

Location 15—West Nephi

Location 15—West Nephi

Location 16—Mona

Location 16—Mona

Location 17–Levan

Location 17–Levan

Location 18—Chicken Creek Res.

Location 18—Chicken Creek Res.

Location 19—Mills Valley

Location 19—Mills Valley

Location 20–Delta

Location 20–Delta

Location 21—Fillmore.

Location 21—Fillmore

Location 22—Kanosh

Location 22—Kanosh

Location 23—Scipio

Location 23—Scipio